A crescent-shaped ALIX dimer targets ESCRT-III CHMP4 filaments.

Ricardo Pires, Bettina Hartlieb, Luca Signor, Guy Schoehn, Suman Lata,
Manfred Roessle, Christine Moriscot, Sergei Popov, Andreas Hinz, Marc
Jamin, et al.

1

A crescent shaped ALIX dimer targets ESCRT-III CHMP4 filaments

R. Pires[1,7], B. Hartlieb[1,7], L. Signor[2], G. Schoehn[1,2], S. Lata[1], M. Roessle[3], C. Moriscot[1,2],

S. Popov[5], A. Hinz[1], M. Jamin[1], V. Boyer[1], R. Sadoul[4], E. Forest[2], D. I. Svergun[3] , H. G.

Göttlinger[5] and W. Weissenhorn[1,6]

[1]Unit of Virus Host Cell Interactions (UVHCI) UMI 3265 Université Joseph Fourier-EMBL-CNRS, 6 rue Jules Horowitz 38042 Grenoble Cedex 9, France

[2] Institut de Biologie Structurale Jean-Pierre Ebel, UMR 5075 CEA-CNRS-UJF, 41, rue Jules Horowitz, 38027 Grenoble cedex 01, France

[3]European Molecular Biology Laboratory (EMBL), Notkestrasse 85, 22603 Hamburg Germany

[4]Grenoble Institute of Neurosciences, INSERM Unit 387 and Université Joseph Fourier, Grenoble I, F-38043 Grenoble, France

[5]Program in Gene Function and Expression, Program in Molecular Medicine, University of Massachusetts Medical School, Worcester, MA 01605, USA

[7]contributed equally

[6]Corresponding author: e-mail: weissenhorn@embl.fr
                          Tel: 33-476-207281
                          Fax: 33-476-209400

Characters with space 54,726

Abstract

ALIX recruits ESCRT-III CHMP4 and is involved in membrane remodeling during endosomal receptor sorting, budding of some enveloped viruses and cytokinesis. We show that ALIX dimerizes via the middle domain (ALIX$_{-V}$) in solution. Structural modeling based on small angle X-ray scattering (SAXS) data reveal an elongated crescent shaped conformation for dimeric ALIX lacking the proline rich domain (ALIX$_{BRO1-V}$). Mutations at the dimerization interface prevent dimerization and induce an open elongated monomeric conformation of ALIX$_{-V}$ as determined by SAXS modeling. ALIX dimerizes *in vivo* and dimeric ALIX co-localizes with CHMP4B upon co-expression. We show further that ALIX dimerization affects HIV-1 budding. C-terminally truncated activated CHMP4B retaining the ALIX binding site forms linear, circular and helical filaments *in vitro*, which can be bridged by ALIX. Our data suggest that dimeric ALIX represents the active form that interacts with ESCRT-III CHMP4 polymers and functions as a scaffolding protein during membrane remodeling processes.

Introduction

Endosomal sorting processes determine the fate of plasma membrane receptors that are either recycled or delivered to the lysosome for degradation. (Gruenberg and Stenmark, 2004; Hicke, 2001; Katzmann et al., 2002). An intricate network of protein interactions, which includes the sequential recruitment of ESCRT (Endosomal Sorting Complexes Required for Transport) complexes 0, I, II and III and associated molecules, regulates endosomal protein sorting, vesicle formation and budding (Saksena et al., 2007) (Hurley, 2008)(Lata et al., 2009). The accessory protein ALIX interacts with ESCRT-I Tsg101 (Mahul-Mellier et al., 2006; Strack et al., 2003) as well as with all ESCRT-III CHMP4 isoforms (Odorizzi et al., 2003)(Katoh et al., 2003)(Fisher et al., 2007)(McCullough et al., 2008). ESCRT-III proteins polymerize on membranes (Babst et al., 2002)(Lin et al., 2005) by forming filamentous (Ghazi-Tabatabai et al., 2008), circular (Hanson et al., 2008) and helical tubular structures (Lata et al., 2008b) that act during membrane remodeling processes including membrane abscission (Lata et al., 2009). ESCRT-III proteins form inactive closed conformations in the cytosol and undergo polymerization and membrane targeting upon activation (Muziol et al., 2006)(Zamborlini et al., 2006)(Shim et al., 2007)(Lata et al., 2008a)(Lata et al., 2008b). It is most likely that ALIX interacts only with an activated form of CHMP4 via a C-terminal CHMP4 binding motif (McCullough et al., 2008). Thus ALIX function must be linked to the role of ESCRT-III in membrane remodeling processes. In fact, ALIX itself might directly control changes in membrane structures (Matsuo et al., 2004)(Falguieres et al., 2008).

ALIX was originally thought to be a homologue of yeast Bro1 that functions in receptor down regulation (Odorizzi et al., 2003)(Kim et al., 2005), but this role could not be confirmed (Cabezas et al., 2005)(Schmidt et al., 2004)(Doyotte et al., 2008).

ALIX is recruited to the budding process of some enveloped viruses such as HIV-1 and equine infectious anemia virus (EIAV) (von Schwedler et al., 2003)(Strack et al., 2003)(Martin-Serrano et al., 2003). Although EIAV budding is strictly dependent on ALIX (Martin-Serrano et al., 2003)(Strack et al., 2003), the EIAV late domain can be replaced by ESCRT-I Vps28, which provides access to ESCRT-III (Tanzi et al., 2003)(Pineda-Molina et al., 2006). In contrast, ALIX is not sufficient to support HIV-1 budding in the absence of the Tsg101/ESCRT-I function (Garrus et al., 2001)(Martin-Serrano et al., 2001). However, over-expression of ALIX or NEDD4 can rescue HIV-1 late domain mutants (Usami et al., 2007)(Chung et al., 2008)(Usami et al., 2008).

Both ALIX and ESCRT-III family members are recruited to the midbody during cytokinesis (Carlton and Martin-Serrano, 2007)(Morita et al., 2007) where ALIX competes with Tsg101 for CEP55 interaction (Lee et al., 2008). Although CEP55 itself is not required for virus budding nor any endosome-related processes, virus budding and cytokinesis require ESCRT-III and VPS4 function.

ALIX is composed of three domains, an N-terminal Bro1-like domain (Kim et al., 2005)(Fisher et al., 2007), which harbors the CHMP4B binding site (McCullough et al., 2008), followed by the V-shaped middle domain composed of two three helical bundles that expose the retroviral late domain binding sites (Lee et al., 2007)(Fisher et al., 2007)(Zhai et al., 2008); the third domain is a proline rich domain (PRD) that serves as a platform for multiple interaction partners including ESCRT-I Tsg101 (von Schwedler et

al., 2003)(Shibata et al., 2004)(Schmidt et al., 2004)(Chatellard-Causse et al., 2002) and CEP55 (Carlton and Martin-Serrano, 2007)(Morita et al., 2007)(Lee et al., 2008). PRD harbors the Alg-2 binding site (Suzuki et al., 2008), which links ALIX to apoptotic processes (Missotten et al., 1999)(Vito et al., 1999)(Trioulier et al., 2004)(Mahul-Mellier et al., 2006)(Mahul-Mellier et al., 2008). The scaffold function of ALIX is further underlined by its control of the actin cytoskeleton (Cabezas et al., 2005; Schmidt et al., 2003)(Pan et al., 2006). Finally PRD regulates the function of ALIX by keeping it in an auto-inhibited state (Zhou et al., 2008b)(Zhou et al., 2008a).

Here we show that ALIX dimerizes *in vitro* and *in vivo* via the V-domain, which helps to explain the dominant negative effect on HIV-1 budding observed for truncated ALIX constructs. We determine a main dimerization interface within the hinge region of the V-domain and present a low resolution model of dimeric ALIX based on SAXS analysis. Electron microscopy data indicate further that dimeric ALIX can bridge CHMP4 filaments. Such a scaffolding function may thus help to position ESCRT-III on membranes and allow recruitment of a variety of effectors via its PRD region.

Results

MALLS and SAXS analysis of ALIX. Both recombinant $ALIX_{Bro1-V}$ and $ALIX_V$ elute from gel filtration columns in two distinct peaks. Analytical size exclusion chromatography in combination with multi angle laser light scattering (MALLS) revealed monomers for $ALIX_{Bro1-V}$ and $ALIX_V$ as expected (Fisher et al., 2007)(Lee et al., 2007) as well as dimeric forms with average molecular weights of 158 ± 3 kDa for $ALIX_{Bro1-V}$ (Figure 1A) and 76 ± 3 kDa for $ALIX_V$ (Figure 1B). The ratio of monomers to dimers

purified from *E. coli* was ~ 5:1 for $ALIX_{Bro1-V}$ and ~ 3:1 for $ALIX_V$. Neither $ALIX_{Bro1-V}$ nor $ALIX_V$ monomers display a concentration dependent equilibrium with their respective dimers. Concentration of $ALIX_{Bro1-V}$ and $ALIX_V$ monomers up to 20 mg/ml did not produce dimers, nor did dilution of dimers produce monomers as judged by gel filtration chromatography in agreement with analytical ultracentrifugation results (Fisher et al., 2007). Thus no dimer to monomer exchange could be observed.

In order to understand the structural basis of ALIX dimerization, both $ALIX_{Bro1-V}$ monomers and dimers were analyzed by small angle X-ray scattering. The scattering intensity patterns corresponding to monomeric and dimeric $ALIX_{Bro1-V}$ are shown in Figures 2A. The Guinier analysis revealed a radius of gyration (Rg) of 40.6 ± 0.1 Å for monomeric and 81.2 ± 0.8 Å for dimeric $ALIX_{Bro1-V}$. Maximal protein dimensions (D_{max}) of ~170 Å for the monomeric $ALIX_{Bro1-V}$ and ~300 Å for dimeric $ALIX_{Bro1-V}$ were found by the distance distribution function p(r) computed by a Fourier transformation of the scattering intensity (Figure 2B). This thus indicated that dimerization produced an elongated shaped $ALIX_{Bro1-V}$. The shapes of the ALIX conformers were determined *ab initio* and reconstructed models of $ALIX_{Bro1-V}$ fit the corresponding experimental data with the discrepancy χ of 1.9 and 1.2. The *ab initio* modeling produced an elongated shape with dimensions of ~ 40 x 60 x 145 Å for monomeric $ALIX_{Bro1-V}$ (Figure 2B, inset), which is largely consistent with the crystal structure of $ALIX_{Bro1-V}$ (Fisher et al., 2007). Comparison of the experimental scattering curve and the one calculated from the $ALIX_{Bro1-V}$ crystal structure revealed a discrepancy χ of 2.7. *Ab initio* modeling of dimeric $ALIX_{Bro1-V}$ yielded a crescent-shaped structure with a distance of ~ 270 Å between the ends spanning the concave surface of the dimer (Figure 2C).

Mapping of the dimer interface. In order to analyze the mode of dimerization, D_2O labeling of $ALIX_{Bro1-V}$ coupled to peptide mapping by mass spectrometry analyses were applied. The resulting peptides were mapped onto the structure of monomeric $ALIX_{Bro1-V}$ and scored depending on an increase or decrease in D_2O labeling. The most pronounced decrease in D_2O labeling was observed for a peptide (aa 637-648) corresponding to a potential hinge region between the two arms of $ALIX_V$ (Fisher et al., 2007)(Lee et al., 2007), suggesting that this region is occluded in dimeric ALIX (Figure 3A). The labeling method also revealed higher accessibilities to D_2O labeling in the dimer as compared to the monomer (Figure S1); this includes one region between the two arms of $ALIX_V$ (helices $\alpha11$ and $\alpha18$), several short helical segments within $ALIX_{Bro1}$ (helices $\alpha4$, $\alpha5$, $\alpha8$ and $\alpha10$) and the long extended conformation spanning the concave surface of $ALIX_{Bro1}$ connecting $\alpha10$ and $\alpha11$ (Figures 3B and S1). The data thus indicate a dimerization interface within $ALIX_V$ and potential conformational flexibility within $ALIX_{Bro1}$.

Generation of an elongated "open" monomeric $ALIX_V$ conformation. In order to analyze the role of the $ALIX_V$ hinge region in dimerization, exposed residues within the segment 638-KMKQSNNE-645, that revealed differences in deuterium incorporation (Figure 3A) were changed to residues 638-**EAAQSYKK**-645 ($ALIX_{Vmut1}$) and to residues 638-KMKQS**YKK**-645 ($ALIX_{Vmut2}$). Size exclusion chromatography (SEC) analyses showed that $ALIX_{Vmut1}$ eluted as a single peak at ~12 ml from a Superdex 200 column, a behavior which is different from the elution profile of $ALIX_V$, which forms monomers and dimers (peaks at ~11.6 and ~13.5 ml) (Figure 4A). SEC of ALIX-V_{mut2} produced two new peaks eluting at ~11.2 and at 12.6 ml (Figure 4A). Applying MALLS, the single peak

of ALIX$_{Vmut1}$ was determined to correspond to a molecular weight of ~ 42 kDa and the two peaks obtained for ALIX$_{Vmut2}$ were determined to correspond to monomeric (~42 kDa) and dimeric forms (~86 kDa) of ALIX$_V$ (Figure 4B). Although ALIX$_{Vmut2}$ can still form dimers, the elution positions determined by SEC indicate that both monomers and dimers exhibit a larger hydrodynamic radius as compared to wild type ALIX$_V$.

Monomeric ALIX$_{Vmut1}$ was further analyzed by small angle X-ray scattering and compared to wild type ALIX$_V$. The Guinier analysis of the scattering curves (Figure 5A) revealed a radius of gyration (Rg) of 53.6 Å, and maximal protein dimensions (D$_{max}$) of ~190Å were calculated by the distance distribution function p(r) for ALIX$_{Vmut1}$ (Figure 5B). Wild type ALIX$_V$ SAXS analysis produced a smaller Rg of 33.4 Å and a smaller Dmax of ~ 125 Å (Figure 5B) confirming that the mutations resulted in an elongated conformation. Comparison of the theoretical scattering curve derived from the ALIX$_V$ crystal structure (pdb 2ojq) and the experimental data (Figure 5A) indicated a high discrepancy $\chi > 5$, suggesting that crystallization locked the V-domain in the observed conformation.

The shape of the ALIX$_{Vmut1}$ was determined *ab initio* and resulted in a 170 Å long conformation (Figure 5C). The reconstructed average model of ALIX$_{Vmut1}$ fit the corresponding experimental data with the discrepancy χ of 1.56 (Figure 5A). The model suggests an open conformation of ALIX$_V$, whereas one arm of ALIX$_V$ needs to rotate ~ 140° to fit the elongated envelope (Figure 5D). The monomeric conformation of ALIX$_{Vmut1}$ indicates that the mutations not only prevent dimerization but may also stabilize an open ALIX$_V$ conformation. Together with the SAXS data on dimeric ALIX$_{Bro1-V}$, these results provide support for a dimerization model, whereas opening of

$ALIX_V$ conformation (as observed in the crystal structures) precedes dimerization. This might entail an anti-parallel association of the $ALIX_V$ arms producing an arrangement that positions the Bro1 domains at the extreme ends of the arch-shaped $ALIX_{Bro1-V}$ dimer model (Figure 5E).

$ALIX_{Bro1-V}$ expression in mammalian cells induces dimerization. We used the split YFP complementation assay to test ALIX dimerization in cells (Michnick et al., 2007). Both N-terminal YFP and C-terminal YFP halves were fused to the C-terminus of $ALIX_{Bro1-V}$ and expressed in HEK293 cells. Fluorescence analyses by confocal microscopy revealed detection of YFP fused to $ALIX_{Bro1-V}$ only when both fusion proteins were co-expressed (Figure 6A, right panel). This thus indicates that $ALIX_{Bro1-V}$ forms dimers when expressed in mammalian cells, which mainly localize to the cytoplasm.

Both $ALIX_V$ monomers and dimers interact with a late domain peptide. In order to determine whether dimeric ALIX might affect enveloped virus budding, isothermal calorimetry was performed to determine the interaction of $ALIX_V$ with a peptide derived from EIAV Gag p9. This revealed equilibrium dissociation constants (K_D) of 5 +/- 0.3 μM for monomeric $ALIX_V$, consistent with the reported interactions of ALIX monomers and retroviral late domains (Fisher et al., 2007; Lee et al., 2007; Zhai et al., 2008) and of 8 +/- 1.2 μM for dimeric $ALIX_V$. Thus dimeric ALIX constitutes a target for retroviral Gag.

ALIX dimerization is important for HIV-1 budding. We tested the effect of ALIX dimerization on HIV-1 budding since RFP-$ALIX_{V-PRD}$ expression has been shown to exert a dominant negative effect on HIV-1 particle release (Strack et al., 2003). Expression of

RFP-ALIX$_{Vmut2-PRD}$ (still able to form dimers in solution) in HIV-1 infected cells had no consequence on the dominant negative effect imposed by RFP-ALIX$_{V-PRD}$. Particle release was similarly reduced as in case of wild type RFP-ALIX$_{V-PRD}$ expression (Figure 7B, left panel, lanes 2 and 3). In contrast, expression of RFP-ALIX$_{Vmut1-PRD}$ reversed the dominant negative effect of the wild type because no effect on particle release was observed (Figure 7A, left panel lane 3). Cellular expression levels of RFP-ALIX$_{V-PRD}$ constructs were comparable (Figure 7C) as well as the presence of intracellular Gag products. This thus indicates that the potential to dimerize is required for this ALIX construct in order to exert a dominant negative effect, which confirms a physiological role for ALIX dimerization.

ALIX binds to CHMP4 polymers. We next analyzed whether ALIX$_{Bro1-V}$ interacts with CHMP4 polymers. Both ALIX$_{Bro1-V}$ conformers are found in the upper fractions of a sucrose gradient consistent with their monodispersity in solution (Figure 8A and B). In contrast, C-terminally deleted CHMP4B fused to MBP (MBP-CHMP4B$_{\Delta C}$) forms polymers found in the bottom fractions of a sucrose gradient (Figure 8C). Since MBP-CHMP4B$_{\Delta C}$ lacks the ALIX binding site, we fused the ALIX binding site motif (McCullough et al., 2008) via a linker to MBP-CHMP4B$_{\Delta C}$ (MBP-CHMP4B$_{\Delta C\_ALIX}$). MBP-CHMP4B$_{\Delta C\_ALIX}$ localizes to the upper and to the bottom fractions of a sucrose gradient (Figure 8D) similar to MBP-CHMP4B$_{\Delta C}$. Removal of MBP by TEV cleavage renders all of CHMP4B$_{\Delta C\_ALIX}$ polymeric and is thus present in the bottom of a sucrose gradient (Figure 8E). Incubation of MBP-CHMP4B$_{\Delta C\_ALIX}$ with either monomeric or dimeric ALIX$_{Bro1-V}$ redistributes ALIX$_{Bro1-V}$ from the upper fractions to the bottom

fractions upon sucrose gradient centrifugation (Figures 8F and G). Since both MBP-CHMP4B$_{\Delta C\_ALIX}$ and ALIX$_{Bro1-V}$ migrate at the same positions on SDS-PAGE their presence is confirmed by western blot analyses (Figure 8H). Similar complex formation is observed when CHMP4B$_{\Delta C\_ALIX}$ (MBP removed by TEV cleavage) is incubated with monomeric or dimeric ALIX$_{Bro1-V}$ (Figure 8 I and J).

The bottom fractions of the single proteins and the complexes were analyzed by negative staining electron microscopy. MBP-CHMP4B$_{\Delta C}$ assembles into ring-like structures of varying diameters (~ 40 to ~ 70 nm) (Figure 9A). The width of the rings measures ~25Å and the length of the potential repeating units is ~40 Å (Figure 9H, left panel). Thicker appearing (~100 Å) more filamentous structures are formed by MBP-tagged CHMP4B$_{\Delta C\_ALIX}$ (Figure 9B). Removal of MBP from CHMP4B$_{\Delta C\_ALIX}$ reveals more defined filaments, which have diameters of ~100 Å (Figure 9C). These filaments can be decorated with monomeric ALIX$_{Bro1-V}$, which render the surface to appear fuzzy (Figure 9D). Dimeric ALIX$_{Bro1-V}$ bridges two CHMP4B$_{\Delta C\_ALIX}$ filaments and generates ladders made up of "legs" of CHMP4B and "rungs" of ALIX$_{Bro1-V}$ (Figure 9E). The rungs are ~400Å wide and are ~100 Å longer than dimeric ALIX$_{Bro1-V}$ in solution since SAXS analysis revealed a D$_{max}$ of ~300Å (Figure 2B). The presence of these structures was further confirmed by cryo electron microscopy imaging. The cryo images reveal ~30 Å thick circular arrays (Figure 9F and S2) and ring-like structures for CHMP4B$_{\Delta C\_ALIX}$ (Figure 9G). The length of a potential repeating unit in the rings measures ~50Å, similar to the negatively stained images (Figure 9H, left and right panel). This thus suggests that the filaments or rings are most likely constructed by a head to tail interaction of single CHMP4B molecules. When these structures are decorated with dimeric ALIX$_{Bro1-V}$ linear

and spiral structures are observed with dimeric $ALIX_{Bro1-V}$ spanning a distance of ~ 450Å, with a spacing of ~50 Å between rungs (Figure 9I). The cryo images also show mostly ladders as observed by negative staining although it cannot be excluded that some cross linking between ladders occurs (Figure S3). The difference in spacing observed by negative staining and cryo EM might be either due to the fact that (i) binding of $ALIX_{Bro1-V}$ is sensitive to the heavy atom solution used for negative staining or due to the fact that (ii) $ALIX_{Bro1-V}$, which is in contact with the carbon is embedded with heavy atom and visualized, a phenomenon observed previously (Gaillard et al., 2008). Each $CHMP4B_{\Delta C\_ALIX}$ monomer extends the ALIX binding site from the predicted core CHMP4 structure by ~30 amino acids that could span up to ~100 Å in an extended conformation. The extension of the ALIX binding site peptide from the CHMP4B polymer and the positions of the CHMP4B binding sites in the $ALIX_{Bro1-V}$ dimer (~230 Å apart) cannot explain the observed spacing between two CHMP4B filaments induced by dimeric $ALIX_{Bro1-V}$ interaction. The flexible linkage of a ~300Å long $ALIX_{Bro1-V}$ dimer would not produce the rather evenly spaced CHMP4 filaments. It is thus conceivable that further conformational changes induced by binding to CHMP4B filaments have to occur that produce longer $ALIX_{Bro1-V}$ dimers as indicated by the electron microscopy images. Such changes might include the long extended conformation spanning the whole concave side of $ALIX_{Bro1}$ and connecting $ALIX_{Bro1}$ helix 10 and $ALIX_V$ helix 11. Notably part of this region becomes more accessible to D_2O exchange in the dimer as compared to the monomer (Figure 3B). The preferred detection of ladders might be explained by conformational constraints imposed by the cross linking of two CHMP4 filaments by

ALIX$_{Bro1-V}$, since the ALIX binding site could be positioned towards the interior of the CHMP4B ladder.

Cellular localization of activated CHMP4B and ALIX$_{Bro1-V}$. To determine whether activated CHMP4B$_{\Delta C\_ALIX}$ localizes to membranes and/or induces membrane remodeling (Hanson et al., 2008) in the absence of other ESCRT factors, CHMP4B$_{\Delta C\_ALIX}$ was expressed with a C-terminal flag-tag in HEK293 cells. Immunostaining revealed that CHMP4B$_{\Delta C\_ALIX}$ concentrates in inclusions that appear to be close to the plasma membrane (Figure 6B) similar to a previous report (Lin et al., 2005); upon co-expression with dimeric ALIX$_{Bro1-V}$ fused to the two YFP Venus halves most of ALIX$_{Bro1-V}$ is also recruited into CHMP4B$_{\Delta C\_ALIX}$ positive inclusions (Figure 6C), thus indicating that dimeric ALIX targets ESCRT-III CHMP4 polymers *in vivo*.

Discussion

ALIX is a cellular adaptor protein that engages in a number of seemingly unrelated processes ranging from endosomal trafficking (Saksena et al., 2007), apoptosis (Vito et al., 1999)(Missotten et al., 1999), cytoskeleton reorganization (Cabezas et al., 2005)(Pan et al., 2006), retrovirus budding (Usami et al. 2009) and cytokinesis (Carlton and Martin-Serrano, 2007)(Morita et al., 2007). Thus ALIX underlies tight regulation that requires the C-terminal proline-rich region (PRD) harboring numerous protein-protein interacting motifs important for function and regulation of Alix (Odorizzi, 2006). PRD keeps ALIX in an auto-inhibited conformation (Zhou et al., 2008b)(Zhou et al., 2008a)(Lazert et al., 2008),which suggests that ALIX has to be activated. Our data

indicate that activation of ALIX induces dimerization. Oligomerization and dimerization of ALIX was observed previously(Munshi et al., 2007)(Fisher et al., 2007), and we confirm that the V-domain is sufficient for dimerization. It is, however, yet unclear which signal induces dimerization *in vitro* and *in vivo*. We show that both $ALIX_{Bro1-V \text{ and }} ALIX_V$ monomers and dimers are stable entities and do not exchange *in vitro* (Fisher et al., 2007).

$ALIX_{Bro1-V}$ contains a Bro1 domain (Kim et al., 2005) and a central V-shaped domain (Fisher et al., 2007)(Lee et al., 2007). Bro1 interacts with ESCRT-III CHMP4 and the V-domain harbors the retroviral late domain binding site (Kim et al., 2005)(Zhai et al., 2008)(McCullough et al., 2008)(Lee et al., 2007). SAXS analyses of dimeric $ALIX_{Bro1-V}$ revealed an elongated $ALIX_{Bro1-V}$ structure that measures ~ twice the length of monomeric $ALIX_{Bro1-V}$. Interestingly, the shape of dimeric $ALIX_{Bro1-V}$ resembles that of BAR domains such as amphipysin (Peter et al., 2004) and endophilin (Weissenhorn, 2005). Although we observe membrane interaction of $ALIX_{Bro1-V}$ *in vitro* (data not shown) no specific membrane remodeling effect could be assigned. Thus, the architecture might be preferentially used to bridge two effector molecules.

Since no concentration dependent equilibrium between monomers and dimers could be detected (Fisher et al., 2007), dimer formation must include specific conformational changes. Hydrogen/deuterium exchange experiments coupled to mass spectrometry peptide mapping revealed several sites of conformational flexibility, notably not only within the V-dimerization domain but also within the Bro1 domain. Such conformational flexibility is consistent with the structure of $ALIX_{Bro1-V}$, which shows that Bro1 and V are connected via a short linker as well as some degree of

flexibility between the two arms of the V domain (Fisher et al., 2007). The mutagenesis studies suggest that the two arms of ALIX$_V$ are connected via a hinge region, which is stabilized in the crystal structure by a salt bridge between K640 and E650, that also hydrogen bonds to N400 (Lee et al., 2007)(Fisher et al., 2007). A set of mutations within this region including K640 destabilized the monomer and in addition prevented dimer formation. Since the hydrogen/deuterium exchange experiments suggest that this region is more protected in dimeric ALIX$_{Bro1-V}$, changes within this region might prevent important dimer contacts. Alternatively, the mutations could artificially stabilize an open monomer conformation that itself prevents dimerization. The latter possibility is supported by the SAXS model of ALIX$_{Vmut1}$ that indicates an elongated form of ALIX$_V$; the crystal structure of ALIX$_V$ would fit into the SAXS envelope when one arm of the V-domain is rotated by ~ 140º. Based on these data we suggest the following dimerization model: Displacement of PRD serves as a first signal to release auto-inhibition (Zhou et al., 2008b)(Zhou et al., 2008a), a second signal then leads to an opening of the V-domain and subsequent anti-parallel dimerization via the V-domain arms (Figure 5E).

Expression of truncated ALIX conformers such ALIX$_{V-PRD}$ and ALIX$_V$ have been shown to induce dominant negative effects on retroviral budding (Strack et al., 2003)(Munshi et al., 2007). We show that such an effect is inhibited in the presence of the dimerization mutations since RFP-ALIX$_{Vmut1-PRD}$ expression is no longer a dominant negative inhibitor of HIV-1 budding. It is thus conceivable that truncated forms of ALIX which retain the V dimerization domain form heterodimers with endogenous ALIX. The function of such mixed dimers might be compromised by the lack of adaptor

protein binding which might position the complex within the correct network of interactions required to trigger down stream effects. Thus $ALIX_{Bro1-Vmut1}$ that no longer dimerizes has no effect on the budding process. The dominant negative effect may further depend on the interaction with Gag, since dimeric $ALIX_V$ interacts with a EIAV late domain peptide with a similar K_d as reported for monomeric $ALIX_V$ (Munshi et al., 2007)(Fisher et al., 2007).

Several lines of evidence suggest that ALIX functions directly on membranes. Firstly, ALIX localizes to the plasma and endosomal membranes (Welsch et al., 2006). Secondly, it plays a role in the formation of internal endosomal membranes in conjunction with lysobiphosphatidic acid (LBPA) (Matsuo et al., 2004). Thirdly, expression of $ALIX_{V-PRD}$ was shown to induce cytoplasmic vacuolization into tubulo-vesicular structures that co-localize with ALIX (Chatellard-Causse et al., 2002); this effect might be also due to the formation of mutant-wild type ALIX heterodimers that lack important binding sites. Fourthly, it is recruited by interaction with ESCRT-III CHMP4, which acts at membranes (Katoh et al., 2003)(von Schwedler et al., 2003)(Strack et al., 2003). ESCRT-III proteins CHMP2A and CHMP3 have been shown to assemble into heteromeric helical polymers that may catalyze late budding steps such as abscission (Lata et al., 2008b). Similarly, ESCRT-III CHMP4 expression in mammalian cells was shown to form circular filaments (Hanson et al., 2008) consistent with ring-like and filamentous structures of CHMP4 observed *in vitro* (Ghazi-Tabatabai et al., 2008). Here we show that activated CHMP4, which most likely requires detachment of the C-terminal MIM domain from the N-terminal core (Shim et al., 2007)(Lata et al., 2008a), forms linear filaments as well as spiral and ring-like

structures. The ring and spiral CHMP4B structures (Figure 9A, F, G) are most likely formed by head to tail interactions of single CHMP4B molecules. Thus CHMP4B polymerization differs from CHMP2A-CHMP3 polymerization since it does not require homo- or heterodimerization. The latter is consistent with the excess of CHMP4 over its potential binding partner CHMP6 present in the yeast ESCRT-III complex (Saksena et al., 2009). The spiral CHMP4B structures observed here might thus reflect the polymer structures observed *in vivo* (Hanson et al., 2008) that drive early steps in HIV-1 assembly and budding (Carlson et al., 2008).

Both ALIX and CHMP4B are present at the midbody (Carlton and Martin-Serrano, 2007)(Morita et al., 2007) and CHMP4-ALIX-CEP55 interactions are essential for midbody formation (Carlton et al., 2008). Since dimeric ALIX$_{Bro1-V}$ bridges preferentially two CHMP4B filaments or spirals *in vitro*, ALIX could support CHMP4 polymer positioning on membranes during viral budding as well as at the midbody supported by CEP55 (Carlton et al., 2008)(Morita et al., 2007). ALIX polymerizes itself (Carlton et al., 2008) whereas dimeric ALIX might constitute the the building block for CHMP4 induced polymerization at budding sites. Because ALIX$_{Bro1-V}$ lacks the multimerization site (Carlton et al., 2008), we do not observe ALIX polymers *in vitro*. Polymerization of ALIX is further supported by the stochiometry of ESCRT-III. ESCRT-III contains multiple copies of CHMP4 (Teis et al., 2008)(Saksena et al., 2009) supporting CHMP4 polymerization which in turn provides multiple binding sites for ALIX polymerization.

The formation and physiological role of ALIX dimers was further proven by using a YFP complementation assay (Michnick et al., 2007). Dimeric ALIX$_{Bro1-V}$-YFP

is mostly found in the cytosol, indicating that dimerization is not sufficient for membrane targeting. When it is expressed together with CHMP4B$_{\Delta C\text{-ALIX}}$ both structures co-localize in large inclusions, demonstrating that polymeric CHMP4B recruits dimeric ALIX *in vivo*. Thus our data suggest that recruitment of activated ESCRT-III CHMP4B entails the function of dimeric ALIX$_{Bro1\text{-}V}$. This might help to position ESCRT-III at sites of membrane remodeling by providing access to the cytoskeleton (Cabezas et al., 2005)(Pan et al., 2006).

Experimental procedures

Protein expression and purification

Cloning, expression, purification and SEC characterization including MALLS of ALIX and CHMP4B constructs is described in the supporting online material (SOM).

Small Angle Scattering Data Collection and Analysis

The synchrotron radiation X-ray scattering data were collected on the X33 SAXS beam line (DESY and EMBL, Hamburg) (Koch and Bordas, 1983; Roessle et al., 2007) and at the ESRF beam line ID02 (Grenoble). A MAR345 image plate with online readout (MarResearch, Germany) was used at a sample - detector distance of 2.4 m covering the range of momentum transfer $0.1 < s < 4.5$ nm^{-1} ($s = 4\pi\ sin(\theta)/\lambda$, where θ is the scattering angle and $\lambda = 0.15$ nm is the X-ray wavelength). The s-axis was calibrated by the scattering pattern of Silver-behenate salt (d-spacing 5.84 nm). The scattering patterns from ALIX$_{Bro1\text{-}V}$ in the monomeric and dimeric phase were measured at protein concentrations of 10.0, 7.4, 5.0 and 2 mg/ml and 2.9, 1.4 and 1.2 mg/ml, respectively.

ALIX$_{Vmut1}$ was measured at a concentration of 7mg/ml at the ESRF (Grenoble) beam line ID02. Further details on SAXS data analysis and model calculation are described in SOM.

Mammalian expression constructs and HIV-1 release assay.

The mammalian expression vector pDSRed2-C1/AIP1$_{\Delta BRO}$, encoding ALIX$_{V-PRD}$, with the N-terminal Bro1-domain replaced by RFP (Strack et al., 2003), was mutated to produce both V-domain dimerization mutants (RFP-ALIX$_{Vmut1-PRD}$ and RFP-ALIX$_{Vmut2-PRD}$) using standard procedures. See SOM for further details.

For indirect immunofluorescence detection of CHMP4B$_{\Delta C\_ALIX}$ its cDNA was cloned with a C-terminal Flag-epitope into the mammalian expression vector pCAGGS by PCR using pBADM41-CHMP4B$_{\Delta C\_ALIX}$ as a template. The plasmid was transfected alone or together with ALIX$_{Bro1-V}$ fused to the N-terminal halve of YFP and the C-terminal halve of YFP in HEK293 cells using TransIT (Mirus) and OptiMem (Invitrogen) according to the manufacturer's instructions. For further details see SOM.

Hydrogen/deuterium (H/D) exchange mass spectrometry (MS)

Deuterium labeling of monomeric and dimeric ALIX$_{Bro1-V}$ was carried out by 20-fold dilution of the protein samples in deuterated buffer (5mM Hepes, 100mM NaCl in D$_2$O, pD 7.6) followed by incubation at 4ºC for different time intervals (from 10 s to 30 min). The reaction was quenched by lowering the pD to 2.1 with 0.1 M HCl solution. Pepsin (Sigma-Aldrich) digestion was performed at 4ºC and pH 2.5 for 2 min in 0.1 M HCl and a protein:protease ratio of 1:1 (*w/w*). Further details are reported in SOM.

Electron microscopy

$CHMP4B_{\Delta C-Alix}$ and $ALIX_{Bro1-V}$ were purified by sucrose gradient centrifugation (Lata et al., 2008b) and samples present in the bottom fractions were analyzed by electron microscopy using negative staining with uranyl acetate or sodium silicotungstate (pH 7.0) (Lata et al., 2008b). For cryo electron microscopy $CHMP4B_{\Delta C-Alix}$ alone or in complex with $ALIX_{Bro1-V}$ the sucrose was removed and 4 μl sample were loaded onto a Quantifoil R2/1 holey grid (Quantifoil Micro Tools GmbH, Germany). The grids were treated and observed using a JEOL 2010 FEG electron microscope (Schoehn et al., 2008).

References

Babst, M., Katzmann, D. J., Estepa-Sabal, E. J., Meerloo, T., and Emr, S. D. (2002). ESCRT-III: An endosome-associated heterooligomeric protein complex required for MVB sorting. Dev Cell *3*, 271-282.

Cabezas, A., Bache, K. G., Brech, A., and Stenmark, H. (2005). Alix regulates cortical actin and the spatial distribution of endosomes. J Cell Sci *118*, 2625-2635.

Carlson, L. A., Briggs, J. A., Glass, B., Riches, J. D., Simon, M. N., Johnson, M. C., Muller, B., Grunewald, K., and Krausslich, H. G. (2008). Three-dimensional analysis of budding sites and released virus suggests a revised model for HIV-1 morphogenesis. Cell Host Microbe *4*, 592-599.

Carlton, J. G., Agromayor, M., and Martin-Serrano, J. (2008). Differential requirements for Alix and ESCRT-III in cytokinesis and HIV-1 release. Proc Natl Acad Sci U S A *105*, 10541-10546.

Carlton, J. G., and Martin-Serrano, J. (2007). Parallels between cytokinesis and retroviral budding: a role for the ESCRT machinery. Science *316*, 1908-1912.

Chatellard-Causse, C., Blot, B., Cristina, N., Torch, S., Missotten, M., and Sadoul, R. (2002). Alix (ALG-2-interacting protein X), a protein involved in apoptosis, binds to endophilins and induces cytoplasmic vacuolization. J Biol Chem *277*, 29108-29115.

Chung, H. Y., Morita, E., von Schwedler, U., Muller, B., Krausslich, H. G., and Sundquist, W. I. (2008). NEDD4L overexpression rescues the release and infectivity of human immunodeficiency virus type 1 constructs lacking PTAP and YPXL late domains. J Virol *82*, 4884-4897.

Doyotte, A., Mironov, A., McKenzie, E., and Woodman, P. (2008). The Bro1-related protein HD-PTP/PTPN23 is required for endosomal cargo sorting and multivesicular body morphogenesis. Proc Natl Acad Sci U S A *105*, 6308-6313.

Falguieres, T., Luyet, P. P., Bissig, C., Scott, C. C., Velluz, M. C., and Gruenberg, J. (2008). In vitro budding of intralumenal vesicles into late endosomes is regulated by Alix and Tsg101. Mol Biol Cell *19*, 4942-4955.

Fisher, R. D., Chung, H. Y., Zhai, Q., Robinson, H., Sundquist, W. I., and Hill, C. P. (2007). Structural and biochemical studies of ALIX/AIP1 and its role in retrovirus budding. Cell *128*, 841-852.

Gaillard, J., Neumann, E., Van Damme, D., Stoppin-Mellet, V., Ebel, C., Barbier, E., Geelen, D., and Vantard, M. (2008). Two microtubule-associated proteins of Arabidopsis MAP65s promote antiparallel microtubule bundling. Mol Biol Cell *19*, 4534-4544.

Garrus, J. E., von Schwedler, U. K., Pornillos, O. W., Morham, S. G., Zavitz, K. H., Wang, H. E., Wettstein, D. A., Stray, K. M., Cote, M., Rich, R. L.*, et al.* (2001). Tsg101 and the vacuolar protein sorting pathway are essential for HIV-1 budding. Cell *107*, 55-65.

Ghazi-Tabatabai, S., Saksena, S., Short, J. M., Pobbati, A. V., Veprintsev, D. B., Crowther, R. A., Emr, S. D., Egelman, E. H., and Williams, R. L. (2008). Structure and disassembly of filaments formed by the ESCRT-III subunit Vps24. Structure *16*, 1345-1356.

Gruenberg, J., and Stenmark, H. (2004). The biogenesis of multivesicular endosomes. Nat Rev Mol Cell Biol *5*, 317-323.

Hanson, P. I., Roth, R., Lin, Y., and Heuser, J. E. (2008). Plasma membrane deformation by circular arrays of ESCRT-III protein filaments. J Cell Biol *180(2)*, 389-402.

Hicke, L. (2001). Protein regulation by monoubiquitin. Nat Rev Mol Cell Biol *2*, 195-201.

Hurley, J. H. (2008). ESCRT complexes and the biogenesis of multivesicular bodies. Curr Opin Cell Biol *20*, 4-11.

Katoh, K., Shibata, H., Suzuki, H., Nara, A., Ishidoh, K., Kominami, E., Yoshimori, T., and Maki, M. (2003). The ALG-2-interacting protein Alix associates with CHMP4b, a human homologue of yeast Snf7 that is involved in multivesicular body sorting. J Biol Chem *278*, 39104-39113.

Katzmann, D. J., Odorizzi, G., and Emr, S. D. (2002). Receptor downregulation and multivesicular-body sorting. Nature Reviews Molecular Cell Biology *3*, 893-905.

Kim, J., Sitaraman, S., Hierro, A., Beach, B. M., Odorizzi, G., and Hurley, J. H. (2005). Structural basis for endosomal targeting by the Bro1 domain. Dev Cell *8*, 937-947.

Koch, M. H. J., and Bordas, J. (1983). X-ray diffraction and scattering on disordered systems using synchrotron radiation. Nucl Instrum Methods *208,*, 461-469.

Lata, S., Roessle, M., Solomons, J., Jamin, M., Gottlinger, H. G., Svergun, D. I., and Weissenhorn, W. (2008a). Structural basis for autoinhibition of ESCRT-III CHMP3. J Mol Biol *378*, 818-827.

Lata, S., Schoehn, G., Jain, A., Pires, R., Piehler, J., Gottlinger, H. G., and Weissenhorn, W. (2008b). Helical structures of ESCRT-III are disassembled by VPS4. Science *321*, 1354-1357.

Lata, S., Schoehn, G., Solomons, J., Pires, R., Gottlinger, H.G. and Weissenhorn, W. (2009) Structure and function of ESCRT-III. *Biochem Soc Trans*, **37**, 156-160.

Lazert, C., Chazal, N., Briant, L., Gerlier, D., and Cortay, J. C. (2008). Refined study of the interaction between HIV-1 p6 late domain and ALIX. Retrovirology *5*, 39.

Lee, H. H., Elia, N., Ghirlando, R., Lippincott-Schwartz, J., and Hurley, J. H. (2008). Midbody targeting of the ESCRT machinery by a noncanonical coiled coil in CEP55. Science *322*, 576-580.

Lee, S., Joshi, A., Nagashima, K., Freed, E. O., and Hurley, J. H. (2007). Structural basis for viral late-domain binding to Alix. Nat Struct Mol Biol *14*, 194-199.

Lin, Y., Kimpler, L. A., Naismith, T. V., Lauer, J. M., and Hanson, P. I. (2005). Interaction of the mammalian endosomal sorting complex required for transport (ESCRT) III protein hSnf7-1 with itself, membranes, and the AAA+ ATPase SKD1. J Biol Chem *280*, 12799-12809.

Mahul-Mellier, A. L., Hemming, F. J., Blot, B., Fraboulet, S., and Sadoul, R. (2006). Alix, making a link between apoptosis-linked gene-2, the endosomal sorting complexes required for transport, and neuronal death in vivo. J Neurosci *26*, 542-549.

Mahul-Mellier, A. L., Strappazzon, F., Petiot, A., Chatellard-Causse, C., Torch, S., Blot, B., Freeman, K., Kuhn, L., Garin, J., Verna, J. M.*, et al.* (2008). Alix and ALG-2 are involved in TNF-R1 induced cell death. J Biol Chem *283(50)*, 34954-65.

Martin-Serrano, J., Yarovoy, A., Perez-Caballero, D., and Bieniasz, P. D. (2003). Divergent retroviral late-budding domains recruit vacuolar protein sorting factors by using alternative adaptor proteins. Proc Natl Acad Sci U S A *100*, 12414-12419.

Martin-Serrano, J., Zang, T., and Bieniasz, P. (2001). HIV-1 and Ebola virus encode small peptide motifs that recruit Tsg101 to sites of particle assembly to facilitate egress. Nat Med *7*, 1313 - 1319.

Matsuo, H., Chevallier, J., Mayran, N., Le Blanc, I., Ferguson, C., Faure, J., Blanc, N. S., Matile, S., Dubochet, J., Sadoul, R., *et al.* (2004). Role of LBPA and Alix in multivesicular liposome formation and endosome organization. Science *303*, 531-534.

McCullough, J., Fisher, R. D., Whitby, F. G., Sundquist, W. I., and Hill, C. P. (2008). ALIX-CHMP4 interactions in the human ESCRT pathway. Proc Nat Acad Sci USA *105*, 7687-7691.

Michnick, S. W., Ear, P. H., Manderson, E. N., Remy, I., and Stefan, E. (2007). Universal strategies in research and drug discovery based on protein-fragment complementation assays. Nat Rev Drug Discov. *6*, 569-582.

Missotten, M., Nichols, A., Rieger, K., and Sadoul, R. (1999). Alix, a novel mouse protein undergoing calcium-dependent interaction with the apoptosis-linked-gene 2 (ALG-2) protein. Cell Death Differ *6*, 124-129.

Morita, E., Sandrin, V., Chung, H. Y., Morham, S. G., Gygi, S. P., Rodesch, C. K., and Sundquist, W. I. (2007). Human ESCRT and ALIX proteins interact with proteins of the midbody and function in cytokinesis. EMBO J *26*, 4215-4227.

Munshi, U. M., Kim, J., Nagashima, K., Hurley, J. H., and Freed, E. O. (2007). An Alix fragment potently inhibits HIV-1 budding: characterization of binding to retroviral YPXL late domains. J Biol Chem *282*, 3847-3855.

Muziol, T., Pineda-Molina, E., Ravelli, R. B., Zamborlini, A., Usami, Y., Gottlinger, H., and Weissenhorn, W. (2006). Structural basis for budding by the ESCRT-III factor CHMP3. Dev Cell *10*, 821-830.

Odorizzi, G. (2006). The multiple personalities of Alix. J Cell Sci *119*, 3025-3032.

Odorizzi, G., Katzmann, D. J., Babst, M., Audhya, A., and Emr, S. D. (2003). Bro1 is an endosome-associated protein that functions in the MVB pathway in Saccharomyces cerevisiae. Journal of Cell Science *116*, 1893-1903.

Pan, S., Wang, R., Zhou, X., He, G., Koomen, J., Kobayashi, R., Sun, L., Corvera, J., Gallick, G. E., and Kuang, J. (2006). Involvement of the conserved adaptor protein Alix in actin cytoskeleton assembly. J Biol Chem *281*, 34640-34650.

Peter, B. J., Kent, H. M., Mills, I. G., Vallis, Y., Butler, P. J. G., Evans, P. R., and McMahon, H. T. (2004). BAR Domains as Sensors of Membrane Curvature: The Amphiphysin BAR Structure. Science *303*, 495-499.

Pineda-Molina, E., Belrhali, H., Piefer, A. J., Akula, I., Bates, P., and Weissenhorn, W. (2006). The crystal structure of the C-terminal domain of Vps28 reveals a conserved surface required for Vps20 recruitment. Traffic *7*, 1007-1016.

Roessle, M. W., Klaering, R., Ristau, U., Robrahn, B., Jahn, D., Gehrmann, T., Konarev, P. V., Round, A., Fiedler, S., Hermes, S., and Svergun, D. I. (2007). Upgrade of the Small Angle X-ray scattering Beamline X33 at the EMBL Hamburg. J Appl Crystallogr 40, 190-194

Saksena, S., Sun, J., Chu, T., and Emr, S. D. (2007). ESCRTing proteins in the endocytic pathway. Trends in Biochemical Sciences *32*, 561-573.

Saksena, S., Wahlman, J., Teis, D., Johnson, A. E., and Emr, S. D. (2009). Functional reconstitution of ESCRT-III assembly and disassembly. Cell *136*, 97-109.

Schmidt, M. H., Chen, B., Randazzo, L. M., and Bogler, O. (2003). SETA/CIN85/Ruk and its binding partner AIP1 associate with diverse cytoskeletal elements, including FAKs, and modulate cell adhesion. J Cell Sci *116*, 2845-2855.

Schmidt, M. H., Hoeller, D., Yu, J., Furnari, F. B., Cavenee, W. K., Dikic, I., and Bogler, O. (2004). Alix/AIP1 antagonizes epidermal growth factor receptor downregulation by the Cbl-SETA/CIN85 complex. Mol Cell Biol *24*, 8981-8993.

Schoehn, G., El Bakkouri, M., Fabry, C. M., Billet, O., Estrozi, L. F., Le, L., Curiel, D. T., Kajava, A. V., Ruigrok, R. W., and Kremer, E. J. (2008). Three-dimensional structure of canine adenovirus serotype 2 capsid. J Virol *82*, 3192-3203.

Shibata, H., Yamada, K., Mizuno, T., Yorikawa, C., Takahashi, H., Satoh, H., Kitaura, Y., and Maki, M. (2004). The penta-EF-hand protein ALG-2 interacts with a region containing PxY repeats in Alix/AIP1, which is required for the subcellular punctate distribution of the amino-terminal truncation form of Alix/AIP1. J Biochem (Tokyo) *135*, 117-128.

Shim, S., Kimpler, L. A., and Hanson, P. I. (2007). Structure/Function Analysis of Four Core ESCRT-III Proteins Reveals Common Regulatory Role for Extreme C-Terminal Domain. Traffic *8*, 1068-1079.

Strack, B., Calistri, A., Popova, E., and Gottlinger, H. (2003). AIP1/ALIX is a binding partner for HIV-1 p6 and EIAV p9 functioning in virus budding. Cell *114*, 689 - 699.

Suzuki, H., Kawasaki, M., Inuzuka, T., Okumura, M., Kakiuchi, T., Shibata, H., Wakatsuki, S., and Maki, M. (2008). Structural basis for Ca2+ -dependent formation of ALG-2/Alix peptide complex: Ca2+/EF3-driven arginine switch mechanism. Structure *16*, 1562-1573.

Tanzi, G. O., Piefer, A. J., and Bates, P. (2003). Equine Infectious Anemia Virus Utilizes Host Vesicular Protein Sorting Machinery during Particle Release. J Virol *77*, 8440-8447.

Teis, D., Saksena, S., and Emr, S. D. (2008). Ordered assembly of the ESCRT-III complex on endosomes is required to sequester cargo during MVB formation. Dev Cell *15*, 578-589.

Trioulier, Y., Torch, S., Blot, B., Cristina, N., Chatellard-Causse, C., Verna, J. M., and Sadoul, R. (2004). Alix, a protein regulating endosomal trafficking, is involved in neuronal death. J Biol Chem *279*, 2046-2052.

Usami, Y., Popov, S., and Gottlinger, H. G. (2007). Potent rescue of human immunodeficiency virus type 1 late domain mutants by ALIX/AIP1 depends on its CHMP4 binding site. J Virol *81*, 6614-6622.

Usami, Y., Popov, S., Popova, E., and Gottlinger, H. G. (2008). Efficient and Specific Rescue of Human Immunodeficiency Virus Type 1 Budding Defects by a Nedd4-like Ubiquitin Ligase. J Virol *82*, 4898-4907.

Usami, Y., Popov, S., Popova, E., Inoue, M., Weissenhorn, W. and H, G.G. (2009) The ESCRT pathway and HIV-1 budding. *Biochem Soc Trans*, **37**, 181-184.

Vito, P., Pellegrini, L., Guiet, C., and D'Adamio, L. (1999). Cloning of AIP1, a novel protein that associates with the apoptosis-linked gene ALG-2 in a Ca2+-dependent reaction. J Biol Chem *274*, 1533-1540.

von Schwedler, U. K., Stuchell, M., Muller, B., Ward, D. M., Chung, H. Y., Morita, E., Wang, H. E., Davis, T., He, G. P., Cimbora, D. M., *et al.* (2003). The protein network of HIV budding. Cell *114*, 701-713.

Weissenhorn, W. (2005). Crystal structure of the endophilin-A1 BAR domain. J Mol Biol *351*, 653-661.

Welsch, S., Habermann, A., Jager, S., Muller, B., Krijnse-Locker, J., and Krausslich, H. G. (2006). Ultrastructural analysis of ESCRT proteins suggests a role for endosome-associated tubular-vesicular membranes in ESCRT function. Traffic *7*, 1551-1566.

Zamborlini, A., Usami, Y., Radoshitzky, S. R., Popova, E., Palu, G., and Gottlinger, H. (2006). Release of autoinhibition converts ESCRT-III components into potent inhibitors of HIV-1 budding. Proc Natl Acad Sci U S A *103*, 19140-19145.

Zhai, Q., Fisher, R. D., Chung, H. Y., Myszka, D. G., Sundquist, W. I., and Hill, C. P. (2008). Structural and functional studies of ALIX interactions with YPX(n)L late domains of HIV-1 and EIAV. Nat Struct Mol Biol *15*, 43-49.

Zhou, X., Pan, S., Sun, L., Corvera, J., Lee, Y. C., Lin, S. H., and Kuang, J. (2008a). The CHMP4b and Src docking sites in the Bro1 domain are autoinhibited in the native state of Alix. Biochem J. *418(2)*, 277-84.

Zhou, X., Pan, S., Sun, L., Corvera, J., Lin, S. H., and Kuang, J. (2008b). The HIV-1 p6/EIAV p9 docking site in Alix is autoinhibited as revealed by a conformation-sensitive anti-Alix monoclonal antibody. Biochem J. *414(2)*, 215-20.

Figure legends

Figure 1. ALIX forms monomers and dimers in solution.

(A) $ALIX_{Bro1-V}$ and (B) $ALIX_V$, analyzed by MALLS indicates molecular weights of ~80 and ~160 kDa for $ALIX_{Bro1-V}$ and ~40 and ~80 kDa for $ALIX_V$; left y-axis, refractive index; the molecular weight is blotted on the right axis in a logarithmic scale; x-axis shows the elution volume of the peaks.

Figure 2. Small angle X-ray scattering analysis of $ALIX_{Bro1-V}$. (A) Experimental scattering intensity patterns obtained for monomeric (dark grey) and dimeric (light grey) $ALIX_{Bro1-V}$ are shown as a function of resolution and after averaging and subtraction of solvent scattering. The scattering intensity patterns calculated from the $ALIX_{Bro1-V}$ monomer and dimer SAXS model with the lowest χ value are shown as black lines.

(B) P(r) function of both monomeric (dark grey) and dimeric (light grey) $ALIX_{Bro1-V}$ (both curves have been adjusted to the same height). The *ab initio* model envelope of monomeric $ALIX_{Bro1-V}$ is shown together with the manually docked $ALIX_{Bro1-V}$ structure (Fisher et al., 2007) as inset.

(C) *Ab initio* modeling of dimeric $ALIX_{Bro1-V}$ reveals a crescent shape model spanning ~ 270 Å; two orientations of the bead model including the molecular envelope are shown.

Figure 3. Mapping of the conformational flexibility of $ALIX_{Bro1-V}$.

Hydrogen/deuterium (H/D) exchange labeling coupled to mass spectrometry analysis was used to determine conformational differences between monomeric and dimeric $ALIX_{Bro1-V}$.

(A) Example of local H/D exchange kinetic for the peptide sequence 637-648. The average mass (M_{avg}) is plotted against D_2O incubation time. This reveals a difference in H/D exchange within this region where dimeric ALIX$_{Bro1-V}$ shows less deuterium exchange compared to monomeric ALIX$_{Bro1-V}$ over a period of 30 min.

(B) The H/D exchange results have been plotted onto the structure of ALIX$_{Bro1-V}$ (Fisher et al., 2007) and the differences in deuteration between monomer and dimer (ΔM_{avg}) are scored according to the following color code: green regions are more protected from H/D exchange in dimeric ALIX$_{Bro1-V}$ while regions shown in red < orange < yellow are less accessible to H/D exchange within monomeric ALIX$_{Bro1-V}$. Regions in blue show similar accessibility between monomeric and dimeric ALIX$_{Bro1-V}$ and regions in grey were not covered by peptide mapping of the deuterated forms.

Figure 4. Mutagenesis of the ALIX$_V$ dimer hinge region generates elongated ALIX$_V$ monomers.

(A) SEC reveals that ALIX$_{Vmut1}$ produces only one peak as compared to wild type ALIX$_V$ and ALIX$_{Vmut2.}$

(B) MALLS analyses show that ALIX$_{Vmut1}$ is monomeric and ALIX$_{Vmut2}$ exists in monomer and dimer conformations. Both refractive index and molecular weight analyses (logarithmic scale) are plotted against the elution volume. The molecular weight distribution across each peak is indicated by dots.

Figure 5. SAXS model of ALIX$_{Vmut1}$. (A) X-ray scattering curves of wild type ALIX$_V$ (red) and ALIX$_{Vmut1}$ (blue) is shown after averaging and subtraction of solvent scattering.

The inset shows the corresponding Guinier plots. The theoretical scattering profiles calculated from the *ab initio* models with the lowest χ values are shown as black lines.

(B) P(r) functions of both wild type and mutant $ALIX_{Vmut1}$. (C) *Ab initio* calculated model of $ALIX_{Vmut1}$ reveals an elongated 170Å long rod-like structure; two orientations of the bead models plus envelopes (grey) rotated by 90° are shown. (D) The three helical bundle structure (red ribbon) of one arm of $ALIX_V$ fits into the molecular envelope of $ALIXV_{mut1}$ and the second arm (blue) would fit after a rotation of ~ 140° along the $ALIX_V$ hinge region.

(E) Model for dimeric ALIX. Dimerzation requires that $ALIX_V$ opens and allows anti-parallel interaction of the ALIX V-domains arms.

Figure 6: $ALIX_{Bro1-V}$ dimerizes *in vivo*. $ALIX_{Bro1-V}$ was expressed using a split YFP expression system. (A) Co-expression of both $ALIX_{Bro1-V}$ YFP fusion protein halves in HEK293 cells resulted in complementation (right panel). $ALIX_{Bro1-V}$ expression thus induces $ALIX_{Bro1-V}$ dimerization *in vivo*.

(B) Expression of $CHMP4B_{\Delta C\text{-}ALIX}$ revealed inclusions partly localized along the plasma membrane (left panel).

(C) Co-expression of $ALIX_{Bro1-V}$ YFP fusion constructs and $CHMP4B_{\Delta C\text{-}ALIX}$; red fluorescence $CHMP4B_{\Delta C\text{-}ALIX}$ (left panel), green fluorescence dimeric ALIX (middle panel) and the lower panel show the co-localization: $CHMP4B_{\Delta C\text{-}ALIX}$ recruits $ALIX_{Bro1-V}$ dimers *in vivo* into large inclusions. Control staining with DAPI is shown in all panels.

Figure 7. ALIX dimerization is important for HIV-1 budding. HIV-1 particle release detected upon expression of RFP-ALIX$_{V-PRD}$ wild type and the dimerization mutants.

(A) Expression of RFP-ALIX$_{Vmut1-PRD}$ reverses the dominant negative effect observed for expression of wild type RFP-ALIX$_{V-PRD}$. Lane 1, vector control; lane 2, wild type RFP-ALIX$_{V-PRD}$; lane 3, RFP-ALIX$_{Vmut1-PRD}$. Detection of extracellular Gag levels (virions, left panel) and intracellular Gag levels (right panels) are shown.

(B) Expression of RFP-ALIX$_{Vmut2-PRD}$ does not influence the dominant negative effect observed for expression of wild type RFP-ALIX$_{V-PRD}$. Lane 1, vector control; lane 2, wild type RFP-ALIX$_{V-PRD;}$ lane 3, RFP-ALIX$_{Vmut2-PRD}$.

(C) Expression levels of RFP-ALIX$_{V-PRD}$ are shown for wild type (lane 2) and RFP-ALIX$_{Vmut1-PRD}$ (lane 3) expression (lane 1, RFP vector expression control).

Figure 8. ALIX$_{Bro1-V}$ interacts with CHMP4 polymers *in vitro*. Sucrose gradient centrifugation analysis of monomeric (A) and dimeric (B) ALIX$_{Bro1-V}$, (C) MBP-CHMP4B$_{\Delta C}$, (D) MBP-CHMP4B$_{\Delta C-ALIX}$, (E) CHMP4B$_{\Delta C-ALIX}$, (F) MBP-CHMP4B$_{\Delta C-ALIX}$ and monomeric ALIX$_{Bro1-V}$, (G) MBP-CHMP4B$_{\Delta C-ALIX}$ and dimeric ALIX$_{Bro1-V}$, (H) Western blot detection of both MBP-CHMP4B$_{\Delta C-ALIX}$ and ALIX$_{Bro1-V}$ present in the bottom fraction of gradients F and G; (I) CHMP4B$_{\Delta C-ALIX}$ and monomeric ALIX$_{Bro1-V}$, (J) CHMP4B$_{\Delta C-ALIX}$ and dimeric ALIX$_{Bro1-V}$. (Protein bands migrating below the 50kDa marker protein correspond to MBP* (*; C, D, E, F, G, I, J)).

Figure 9. Electron microscopy analyses of CHMP4B$_{\Delta C-ALIX}$ and ALIX$_{Bro1-V}$ complexes. Negative staining EM images of (A) MBP-CHMP4B$_{\Delta C}$, (B) MBP-

CHMP4B$_{\Delta C\text{-}ALIX}$, (C) CHMP4B$_{\Delta C\text{-}ALIX}$, (D) CHMP4B$_{\Delta C\text{-}ALIX}$ - ALIX$_{Bro1\text{-}V}$ (monomer) complexes, (E) CHMP4B$_{\Delta C\text{-}ALIX}$- ALIX$_{Bro1\text{-}V}$ (dimer) complexes. (F) Cryo-electron microscopy image of CHMP4B$_{\Delta C\text{-}ALIX}$. (G) Cryo EM images of selected ring structures of CHMP4B$_{\Delta C\text{-}ALIX}$; (H) Ring-like structures revealing the potential repeating unit, marked by arrows (left panel, negative staining, right panel cryo image). (I) 5 panels of cryo EM images showing CHMP4B$_{\Delta C\text{-}ALIX}$ - ALIX$_{Bro1\text{-}V}$ (dimer) complexes. The length of one rung and the distance between rungs are indicated schematically in panel 2. The scale bars are 50 nm (A), 100 nm (B-F, I) and 30 nm (G, H).
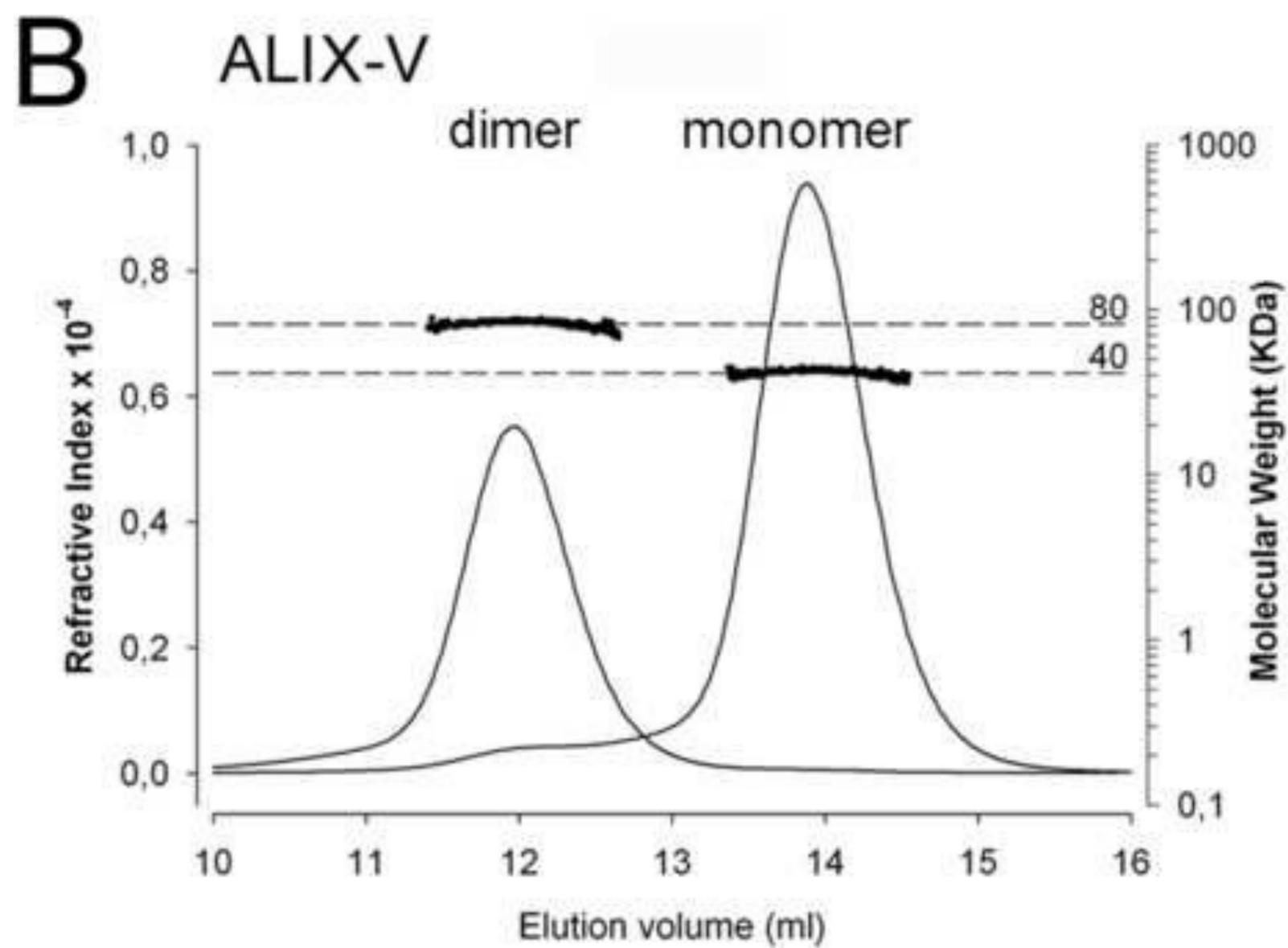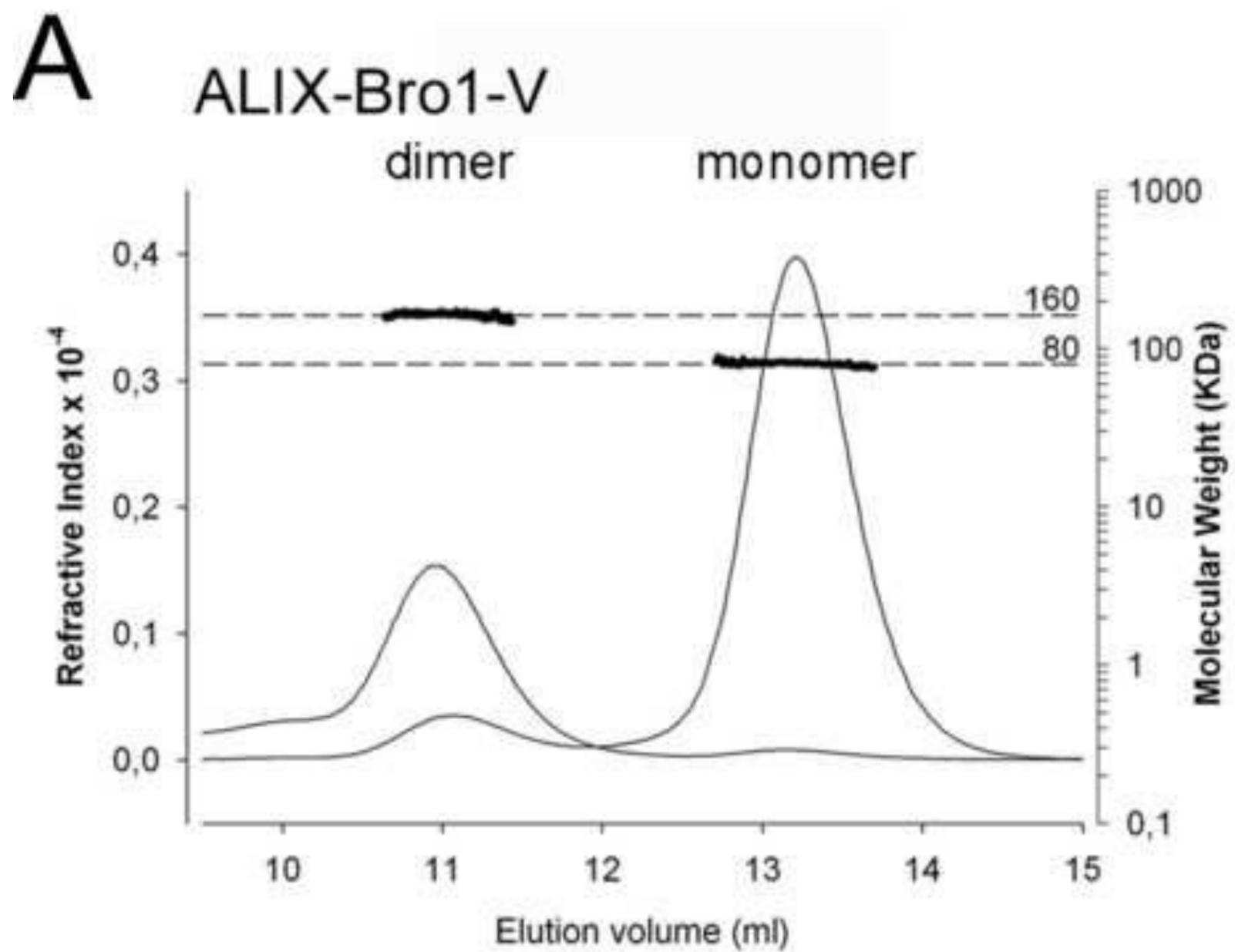
Figure 2
[Click here to download high resolution image](#)
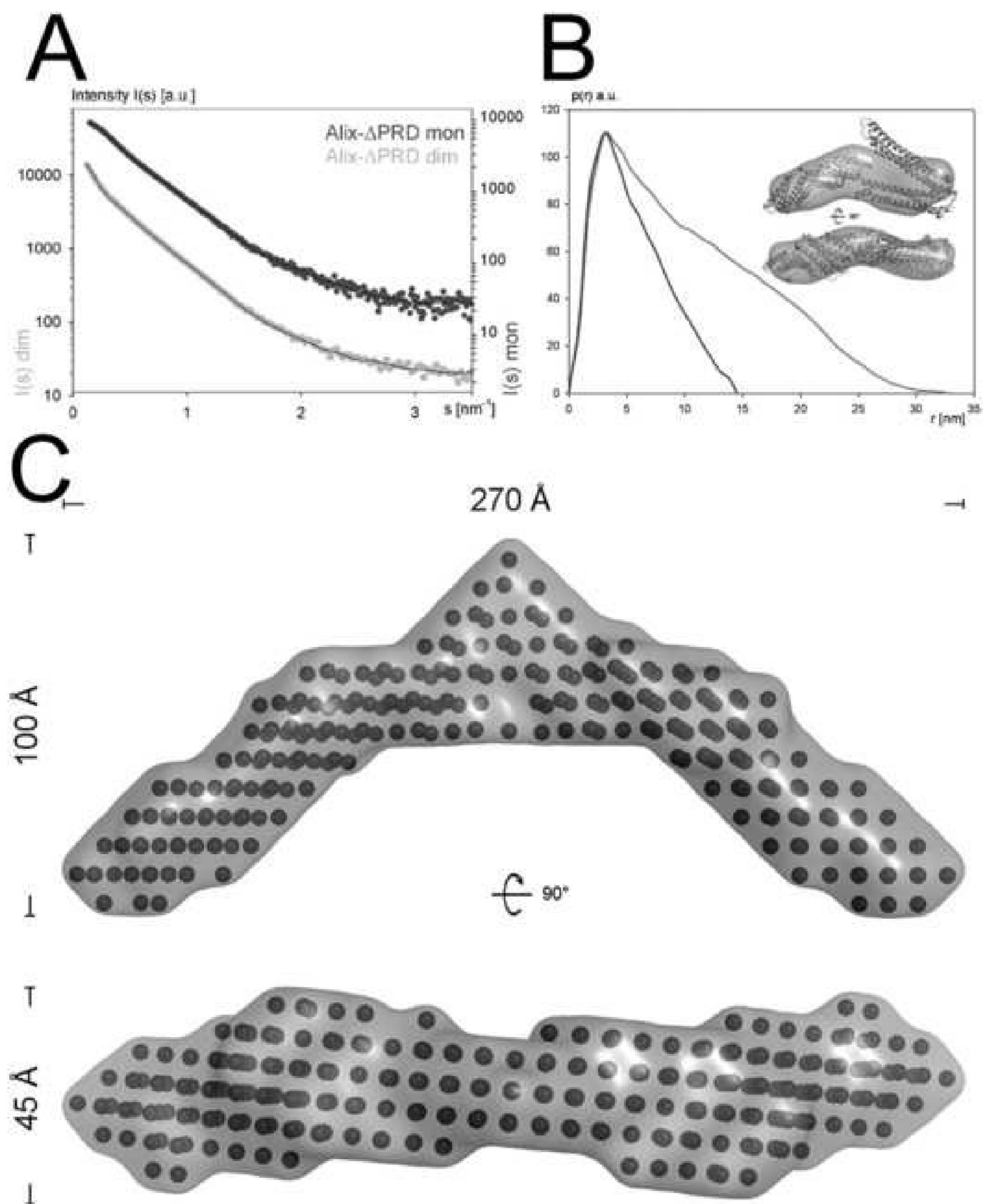
Figure 3
Click here to download high resolution image
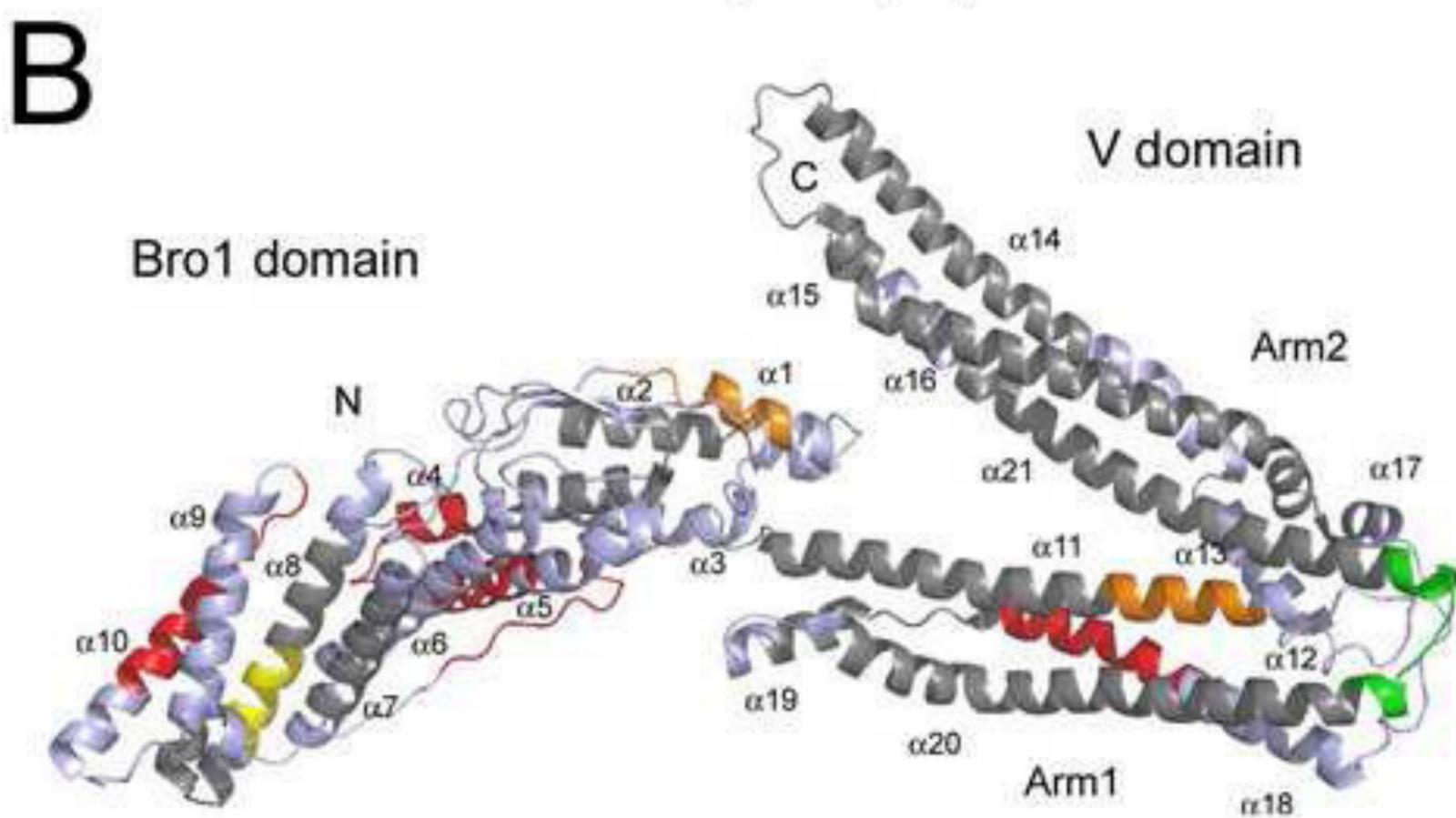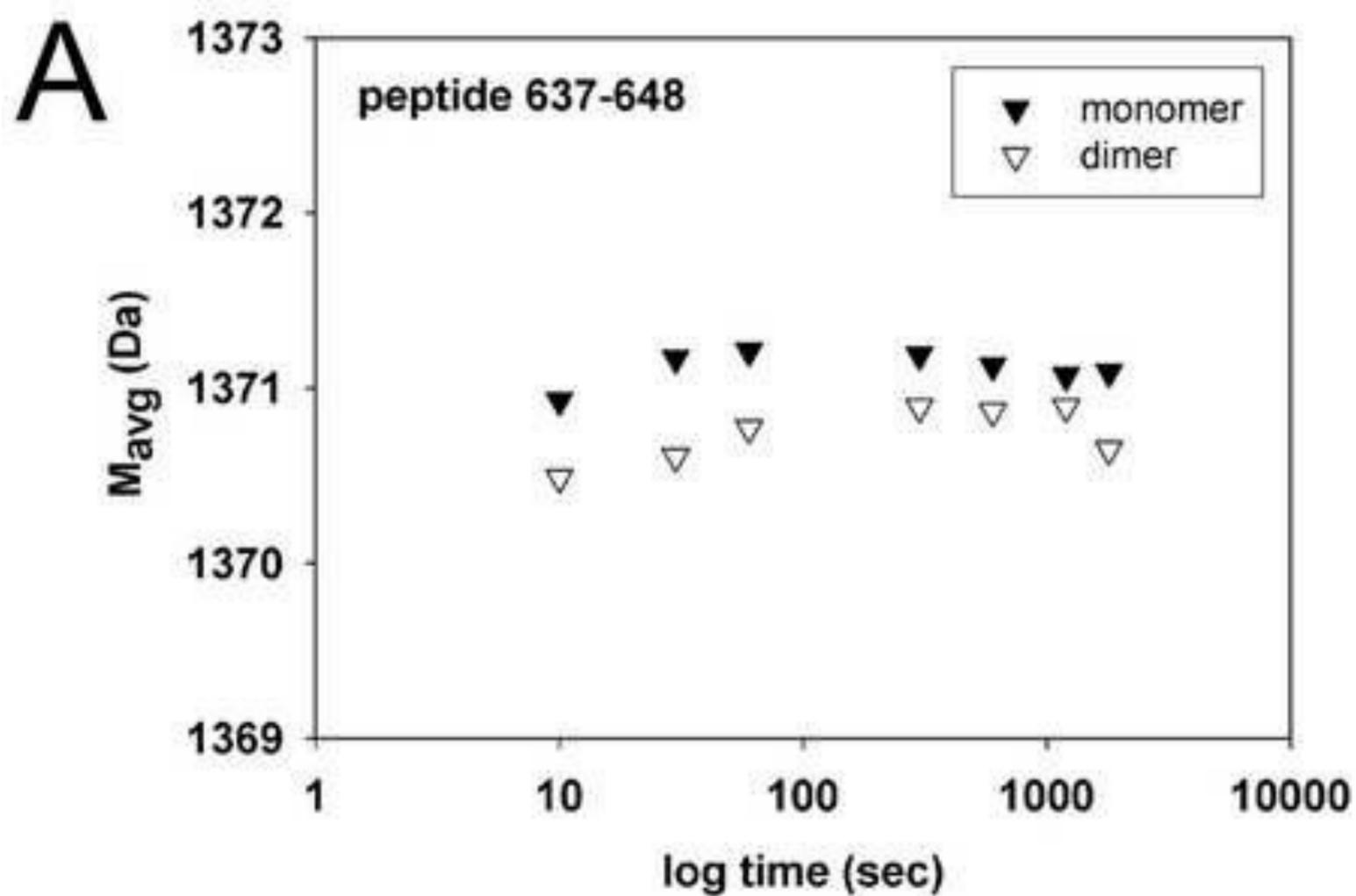
Figure 4
Click here to download high resolution image
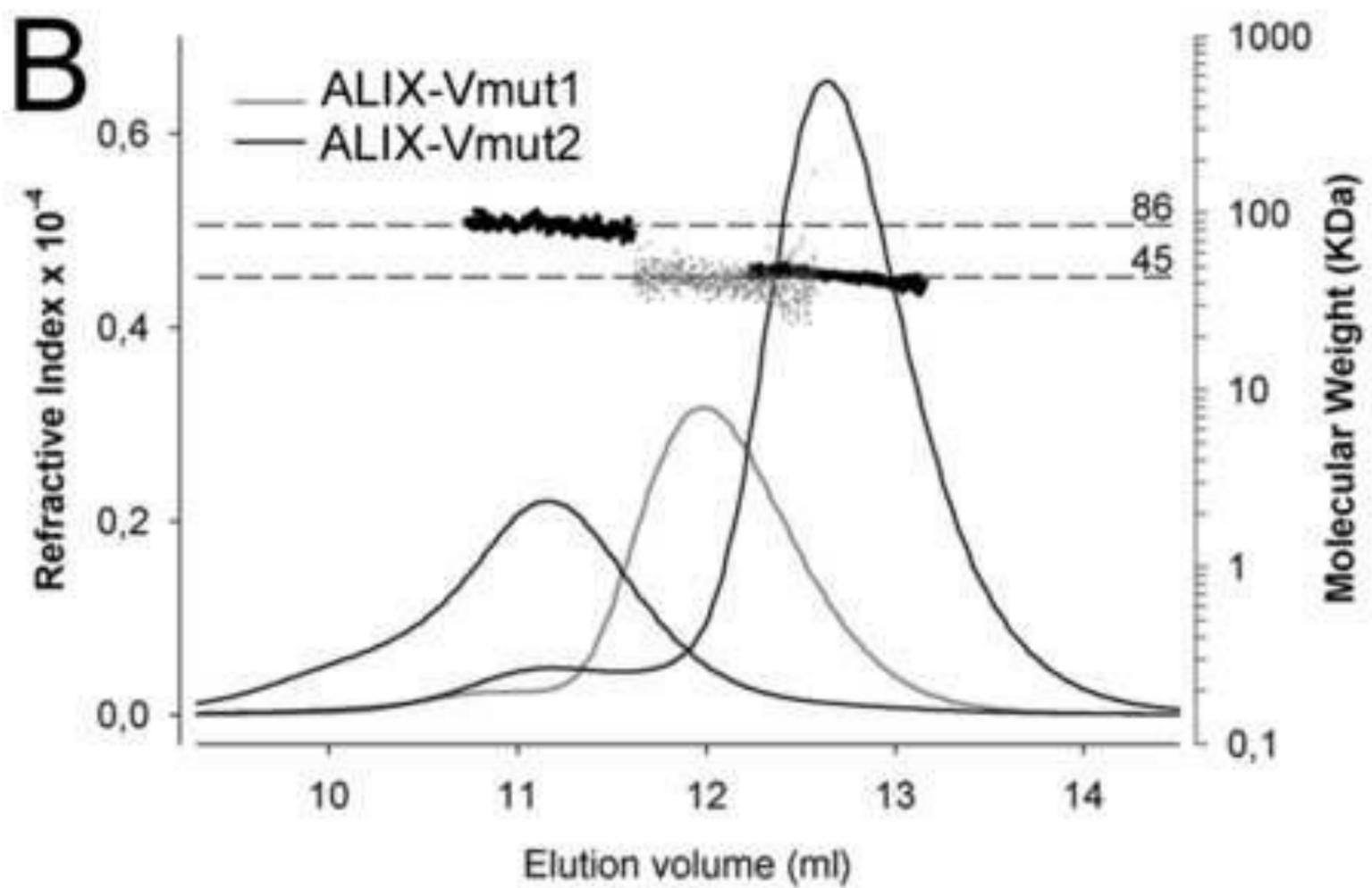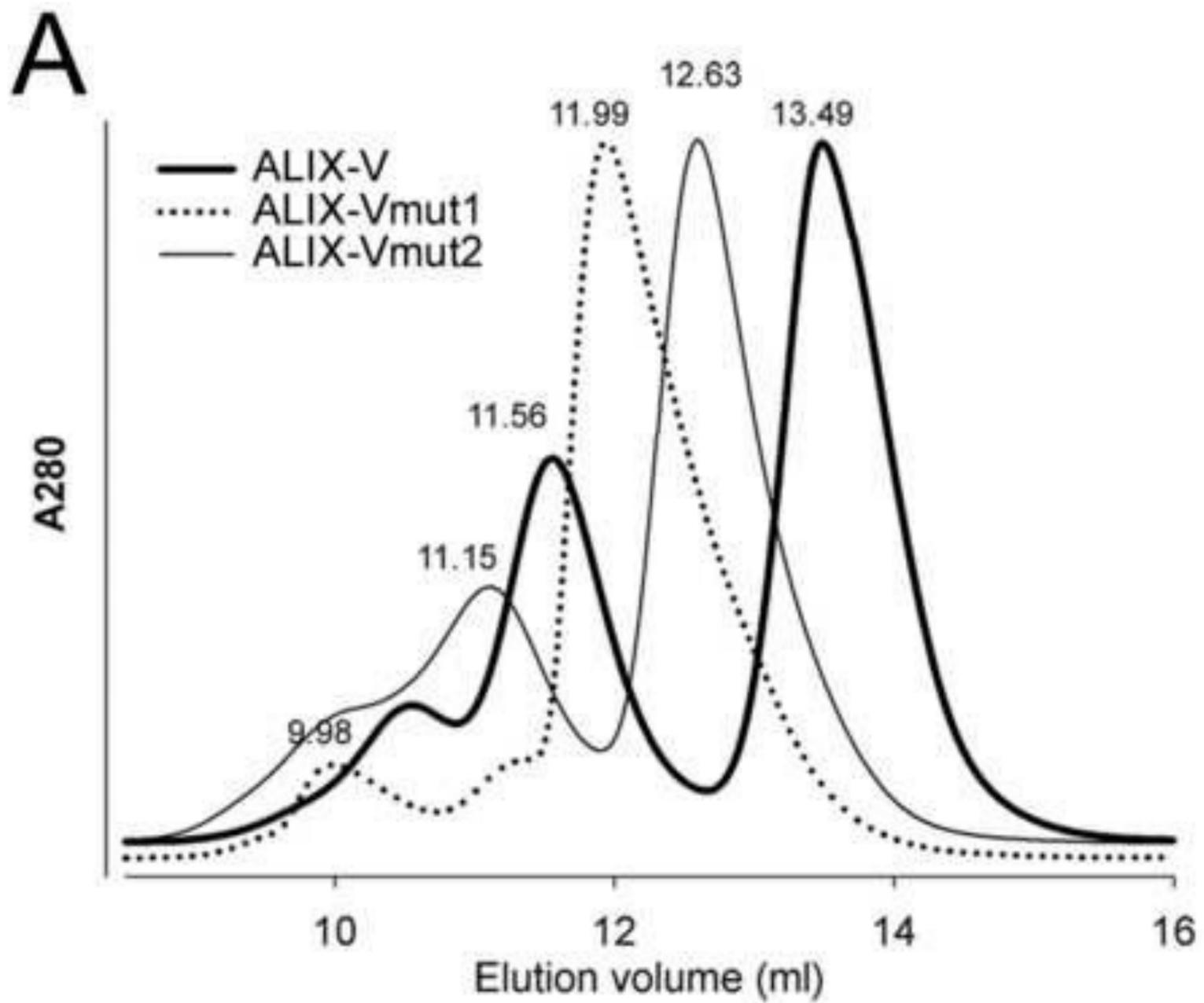
Figure 5
[Click here to download high resolution image](#)

Alexa 596   YFP

A: ALIXBro1-V-YFPNterm +ALIXBro1-V-YFPCterm

B: CHMP4B$_{\Delta C\_ALIX}$

C: CHMP4B$_{\Delta C\_ALIX}$ +ALIXBro1-V-YFPNterm +ALIXBro1-V-YFPCterm
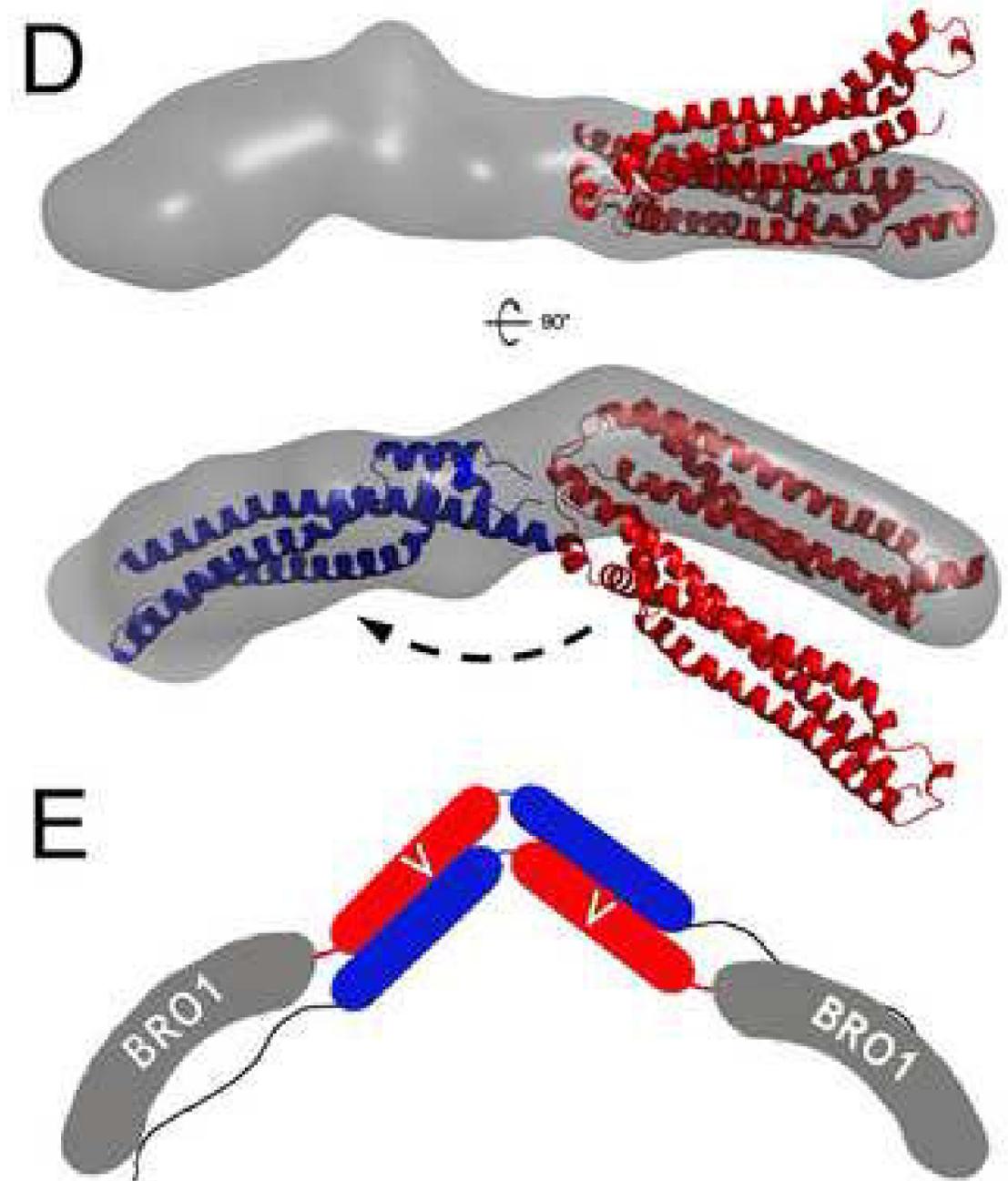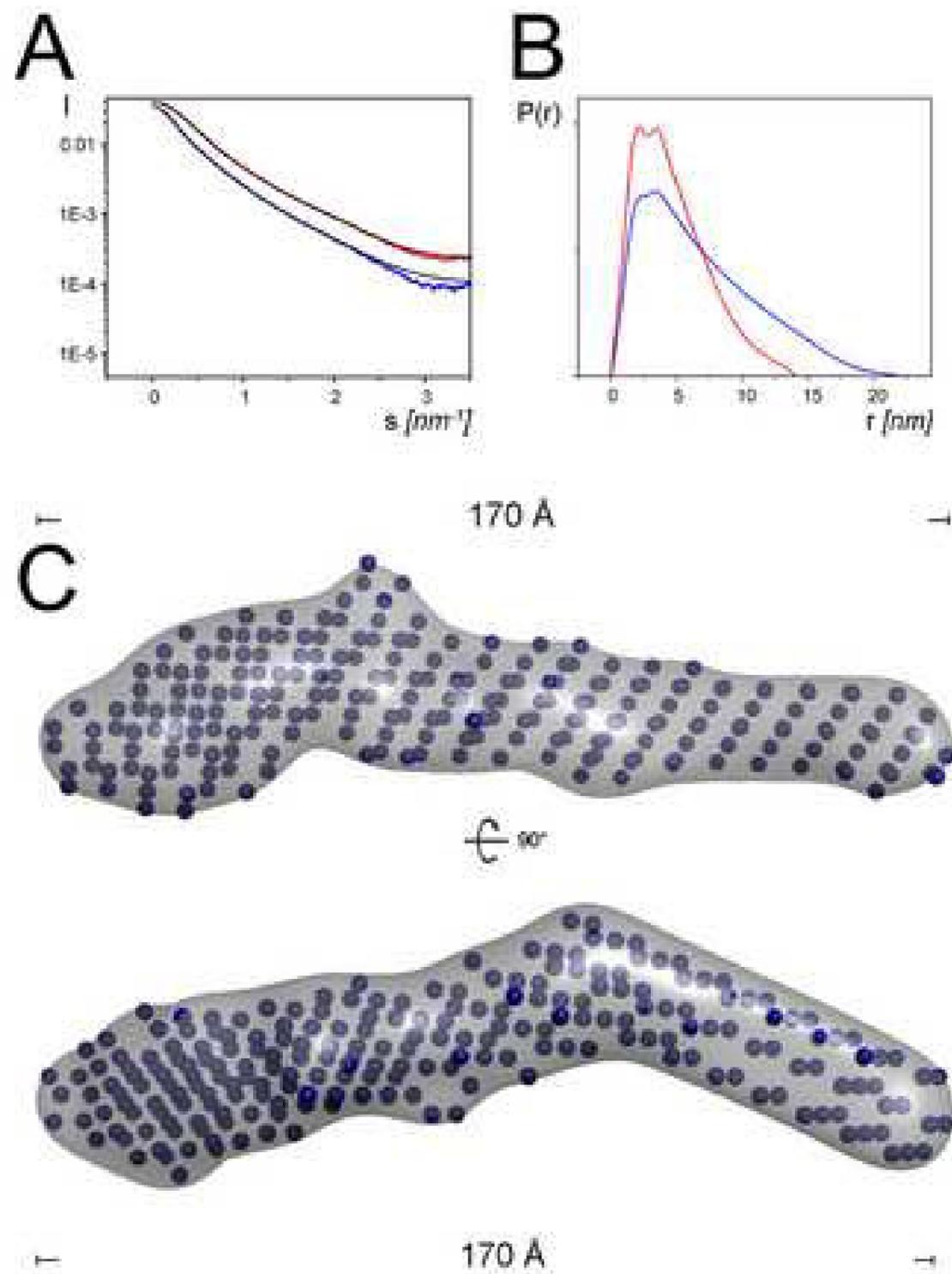
MERGE
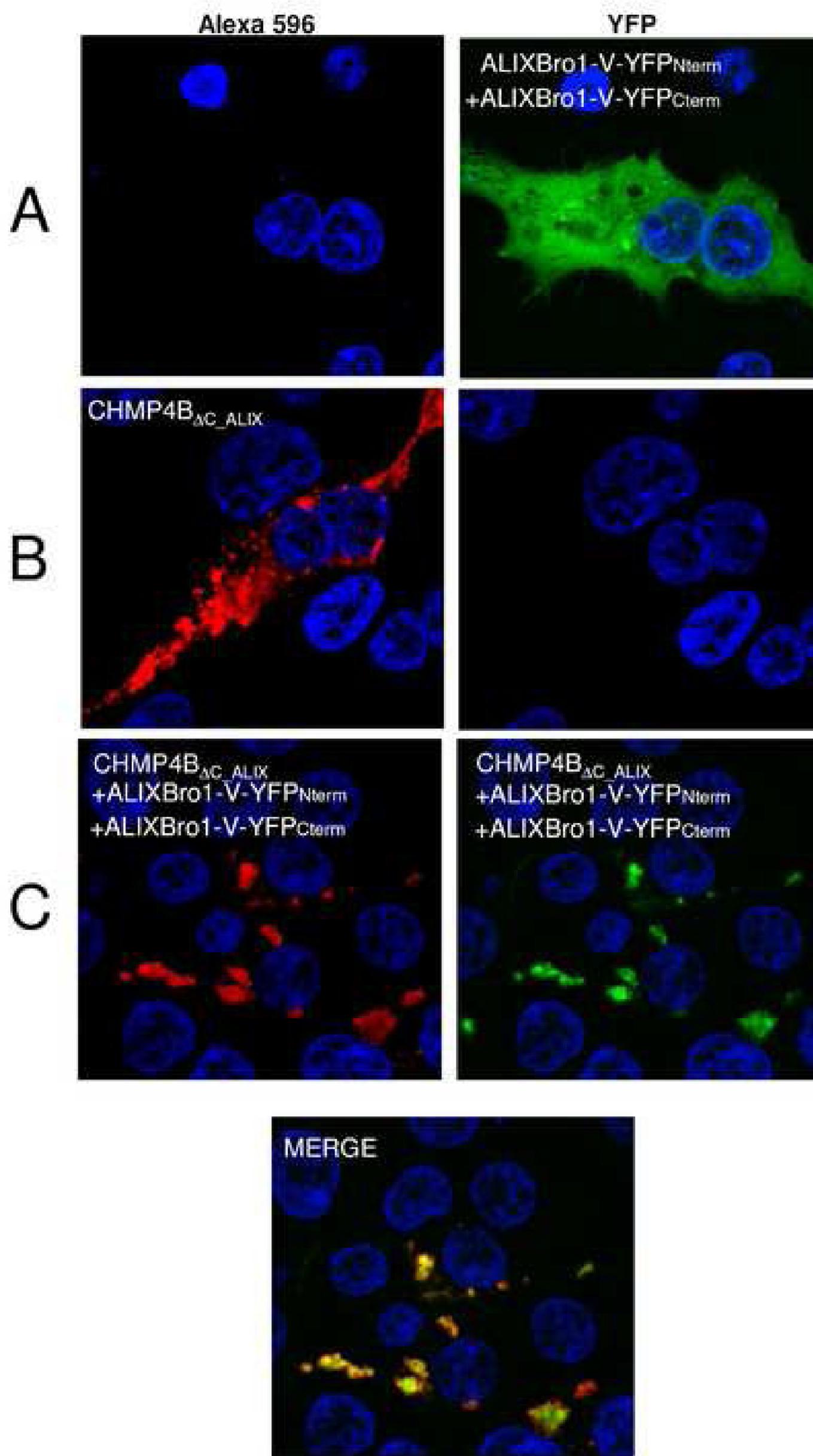
Figure 7
Click here to download high resolution image
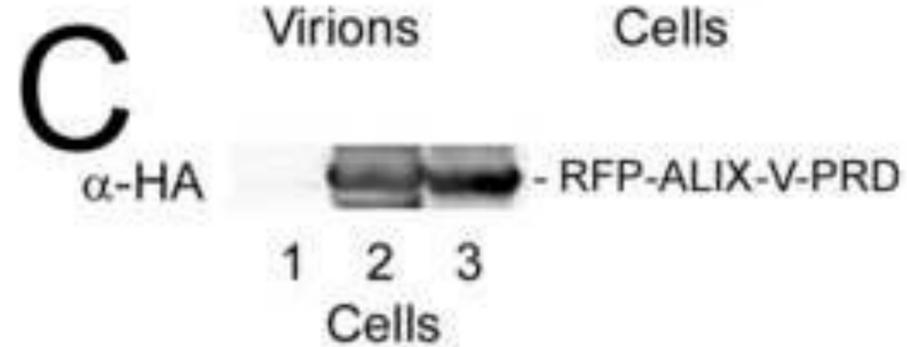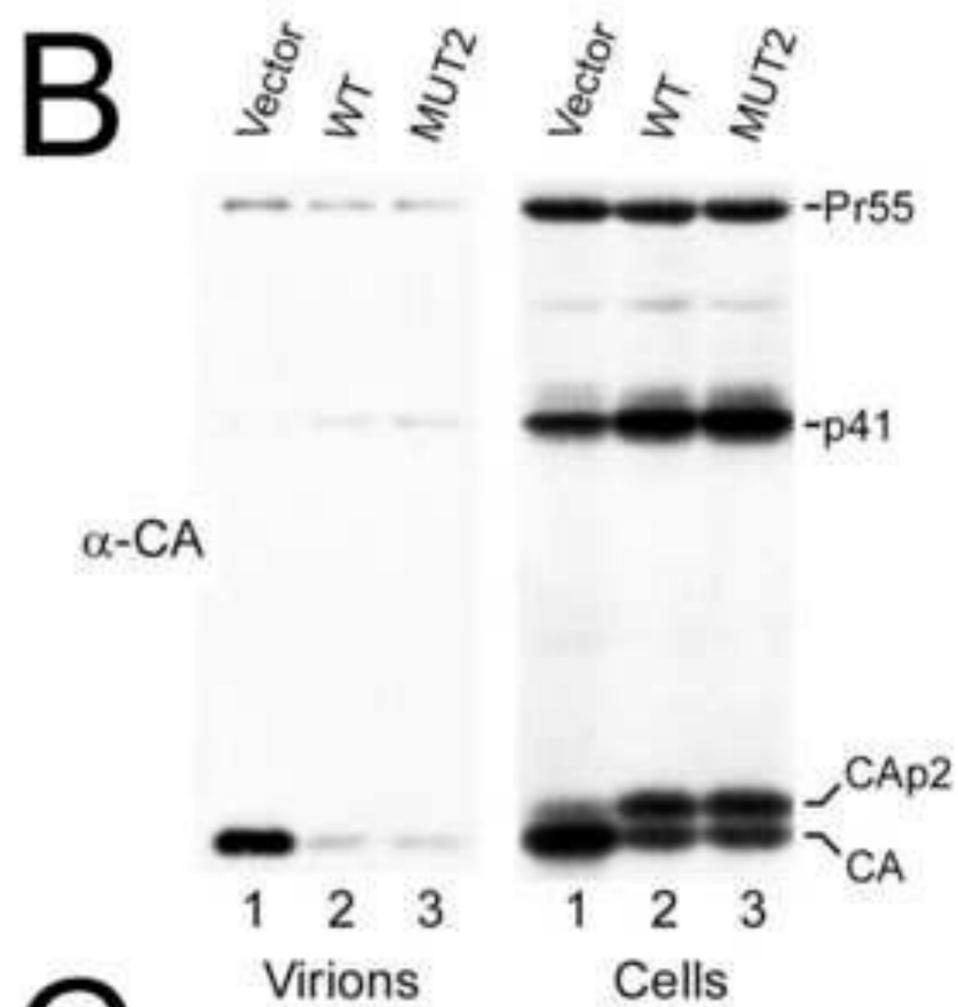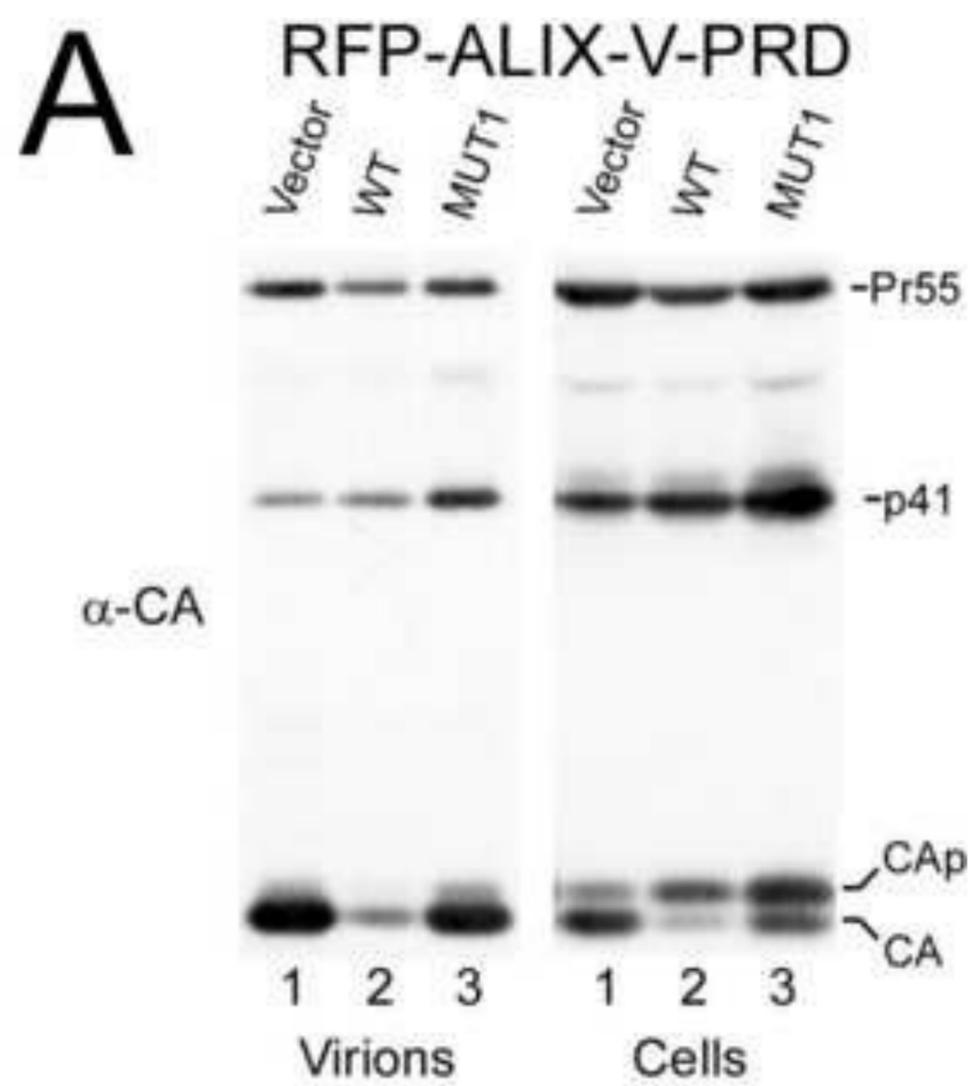
Figure 8
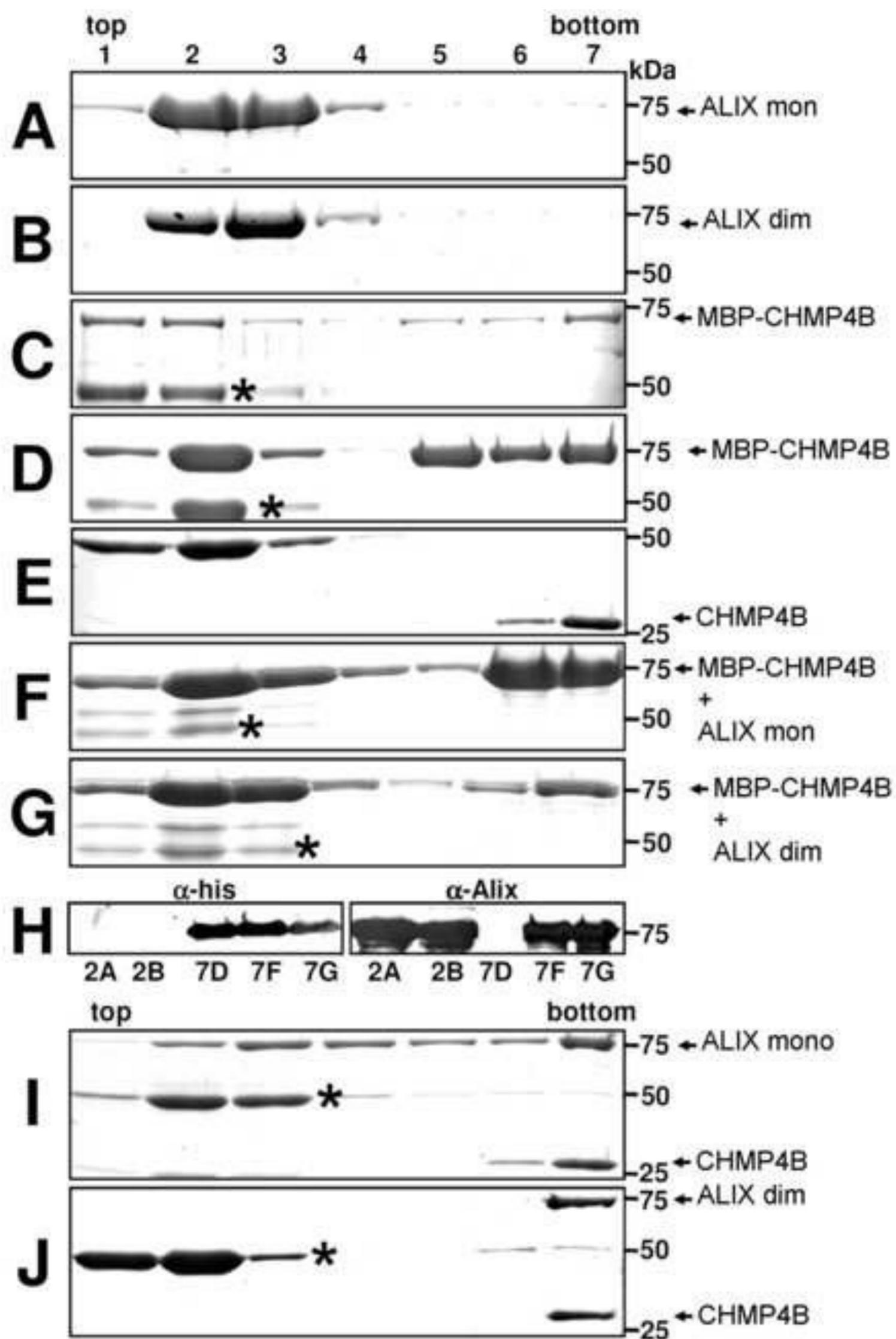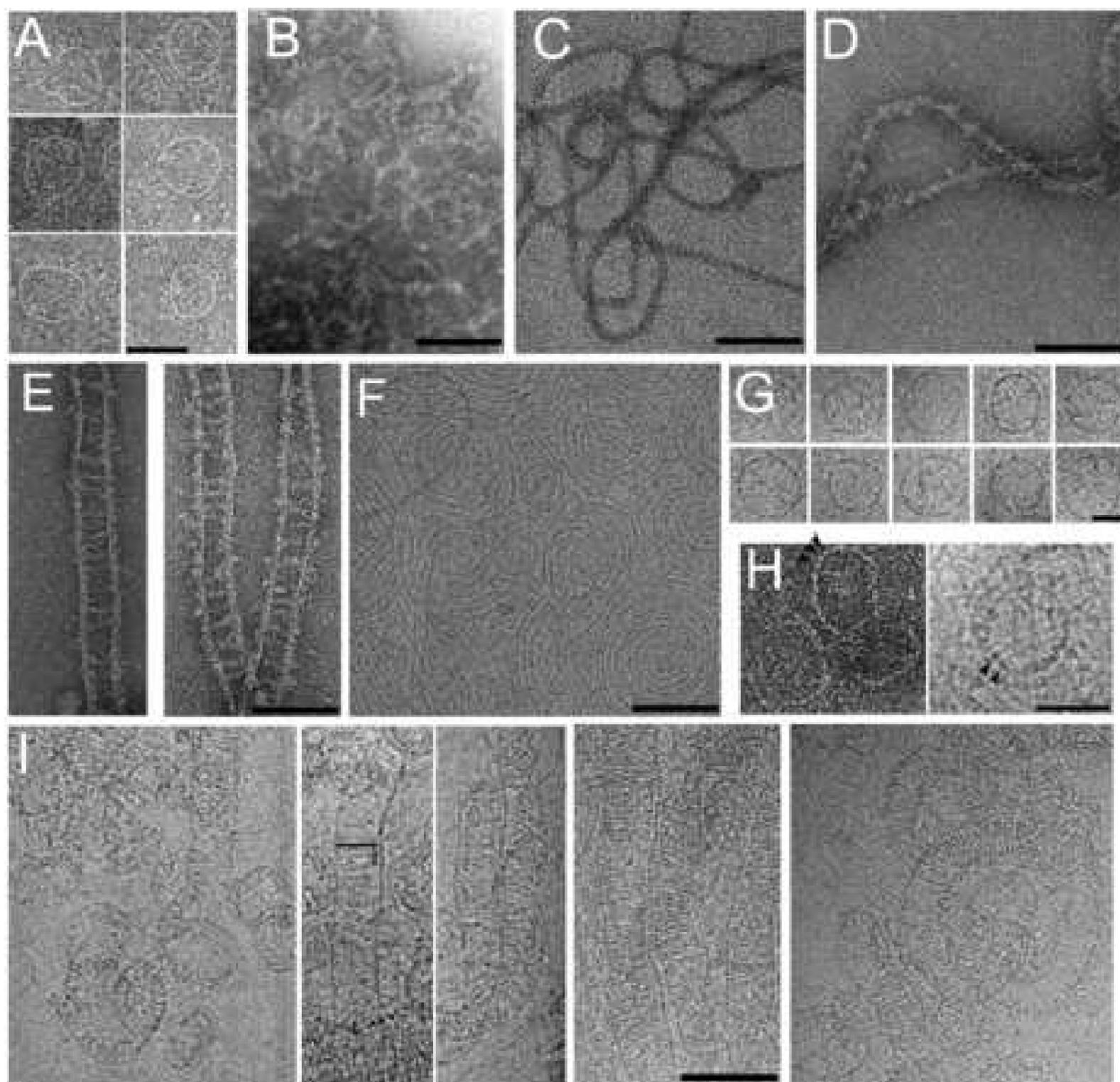
Supporting Online Material for

A crescent shaped ALIX dimer targets ESCRT-III CHMP4 filaments

R. Pires[1,7], B. Hartlieb[1,7], L. Signor[2], G. Schoehn[1,2], S. Lata[1], M. Roessle[3], C. Moriscot[1,2],

S. Popov[5], A. Hinz[1], M. Jamin[1], V. Boyer[1], R. Sadoul[4], E. Forest[2], D. I. Svergun[3], H. G.

Göttlinger[5] and W. Weissenhorn[1,6]

[1]Unit of Virus Host Cell Interactions (UVHCI) UMI 3265 Université Joseph Fourier-EMBL-CNRS, 6 rue Jules Horowitz 38042 Grenoble Cedex 9, France

[2] Institut de Biologie Structurale Jean-Pierre Ebel, UMR 5075 CEA-CNRS-UJF, 41, rue Jules Horowitz, 38027 Grenoble cedex 01, France

[3]European Molecular Biology Laboratory (EMBL), Notkestrasse 85, 22603 Hamburg Germany

[4]Grenoble Institute of Neurosciences, INSERM Unit 387 and Université Joseph Fourier, Grenoble I, F-38043 Grenoble, France

[5]Program in Gene Function and Expression, Program in Molecular Medicine, University of Massachusetts Medical School, Worcester, MA 01605, USA

[7]contributed equally

[6]Corresponding author: e-mail: weissenhorn@embl.fr
                            Tel: 33-476-207281
                            Fax: 33-476-209400

Experimental procedures

Protein expression and purification

ALIX$_{Bro1-V}$ containing residues 1-714 were expressed as a GST fusion protein. in *E. coli* BL21 (DE3)-RIL cells. Cells were harvested by centrifugation, suspended in buffer A (50mM Tris-HCl pH 8.0; 80mM NaCl and 2mM β-mercaptoethanol) and lysed by sonication in the presence of protease inhibitors (complete EDTA-free protease inhibitors, Pierce). The cleared supernatant was loaded onto a glutathione sepharose (Amersham Biosciences) column and the column was washed in buffer A followed by extensive washes in buffer A plus 1 M NaCl and 1 M KCl. GST was cleaved off overnight at 4° with Precission Protease (1:200 w/w) and ALIX$_{Bro1-V}$ was purified on a Q-sepharose column (Amersham Biosciences) in buffer A. A Superdex S200 gel filtration column (Pharmacia) was used as a final purification step in buffer B (20 mM Hepes pH 8.0, 100 mM NaCl). Protein concentration was determined by absorbance at 280 nm in a denaturing buffer (6M guanidinium hydrochloride, 0,02M phosphate buffer pH 6.5). ALIX$_V$, containing residues 355-714, was cloned into expression vector pGEX6P-2 using standard PCR methods. The sequence was confirmed by DNA sequencing. Protein expression was performed in *Escherichia coli* BL21 (DE3)-RIL (Invitrogen) and purified as described for ALIX$_{Bro1-V}$.

CHMP4B$_{ΔC}$ and CHMP4B$_{ΔC\_ALIX}$ were cloned into the expression Vector pBADM41 containing an N-terminal HIS-MBP tag. CHMP4B$_{ΔC}$ comprises amino acids (aa) 1-193 and CHMP4B$_{ΔC\_ALIX}$ corresponds to aa 1-175 followed by a linker of 20 aa (*SNSASDDASASASADEDASS)* and CHMP4B residues 204-224. All constructs were verified by sequencing. Protein expression was performed in *E. coli* BL21 (DE3)-RIL

cells (Invitrogen) at 37°C. Cells were lysed by sonication in buffer C (50 mM Tris·HCl, pH 8.0; 100 mM NaCl; 3 mM 2-mercaptoethanol) including complete EDTA-free protease inhibitors (Pierce). The cell lysate was cleared by centrifugation and loaded onto an amylose column (Amersham Biosiences). The column was sequentially washed with buffer C alone, buffer C plus 1 M NaCl, and buffer C plus 1 M KCl. Proteins were eluted by applying 10 mM Maltose in buffer C. MBP was removed by TEV protease cleavage.

Size exclusion chromatography and multi-angle laser scattering

Size exclusion chromatography was performed with a Shodex Protein KW-804 HPLC column (300 mm x 8.0 mm). The column was equilibrated in buffer E (20 mM Tris pH 7.5, 150 mM NaCl) and the runs were perform at 20 °C with a flow rate of 0.8 ml/min. Stokes' radii were determined by calibrating the column with globular proteins of known Stokes' radius. On-line detection was performed by multi-angle laser light scattering (MALLS) using a DAWN-EOS detector (Wyatt Technology Corp., Santa Barbara, CA) equipped with a laser emitting at 690 nm and by refractive index measurement using a RI2000 detector (Schambeck SFD). Light scattering intensities were measured at different angles relative to the incident beam, and analysis of the data was performed with the ASTRA software (Wyatt Technology Corp., Santa Barbara, CA). Weight-averaged (M_w) molecular weights were obtained from the molecular weight distribution across the elution peak as described (Lata et al., 2008).

HIV-1 release assay.

The virus release assays were performed as described (Strack et al., 2003). Briefly, 293T cells (1.2×10^6) were cotransfected with 1.5 µg of HXBH10, which encodes WT HIV-1, and 1 µg of vectors expressing either wild type or mutant versions of RFP-ALIX$_{V-PRD}$, as indicated. Virions were pelleted through 20% sucrose. Virions and cell lysates were analyzed by Western blotting for detection of Gag proteins by using the anti-HIV-1 CA antibody 183-H12-5C.

Mammalian expression constructs

ALIX$_{Bro1-V}$ cDNA was cloned into pcDNA3.1 vectors that contained the N-terminal and C-terminal halves of YFP (Michnick et al., 2007). Single vectors and both vectors together were transfected into HEK293 cells using TransIT (Mirus) and OptiMem (Invitrogen) according to the manufacturer's instructions. For further details see SOM.

For indirect immunofluorescence HEK293 cells expressing ALIX-YFP fusions were cultured on coverslips and fixed with 4% paraformaldehyde for 20 min at 4°C. The cover slips were further incubated with 100 mM glycine in PBS for 10min // 0.2% Triton X-100 in PBS for 7 min / blocking buffer (5 % glycerol, 2 % BSA, 0.2 % Tween20, 0.05 % sodium-acide in PBS) for 20 min at RT. Nuclei were stained with DAPI slides were mounted in Mowiol for confocal microscopy analysis.

HEK293 cells expressing CHMP4B and or ALIX-YFP were fixed as described above followed by the primary antibody (anti-flag rabbit antibody (Sigma)) incubation in blocking buffer for 1h at 20°C. Slides were washed three times with PBS, followed by the secondary antibody (Alexa596 coupled anti-rabbit goat antibody (Invitrogen) in

blocking buffer) incubation at 20°C for 1h. After three washes with PBS, slides were analyzed by confocal microscopy.

Hydrogen/deuterium (H/D) exchange mass spectrometry (MS)

For LC-MS analysis ALIX peptides obtained by protease digestions were loaded on a peptide MacroTrap column (Michrom Bioresources) and desalted using mobile phase A (0.03% (v/v) TFA solution in water) for 1 min at a flow rate of 300 μl/min. Peptide separation was performed on a reverse phase C18 column (1mm×100mm, ID×L; Interchrom) pre-equilibrated at 15% (*v/v*) ACN-0.03% (v/v) TFA in water using a 15 to 40% linear gradient in mobile phase B (95% ACN (*v/v*) containing 0.03% TFA in water) in 45min (for LC-MS experiments) or in 80 min (for LC-MS/MS experiments) and a flow rate of 50 μl/min. All LC-MS and LC-MS/MS analyses were carried out with valves, trap cartridges and columns cooled to ice-bath temperature to minimize deuterium back-exchange. Peptide mapping (LC-MS/MS) were performed on an ion trap mass spectrometer (Esquire 3000+, Bruker Daltonics) connected to a two-pump HPLC system (Shimadzu). Local kinetics of H/D exchange on peptide fragments (LC-MS) were analyzed on a 6210 TOF LC-MS system (Agilent Technologies). The data were processed using the software packages Data Analysis 3.2 (Bruker Daltonics) and Analyst QS 1.1 (Applied Biosystems). The spectra of peptides before deuteration were compared to those obtained after H/D exchange. The sequence coverage of the peptide map obtained from the non-deuterated protein was 85%. The H/D exchange analyses were done on 31 peptides covering 57 % of the sequence.

Small Angle Scattering Data Collection and Analysis

Protein samples were prepared in 20 mM Hepes pH 8.0, 100 mM NaCl. Repetitive measurements of 180 sec at 15 °C of the same protein solution were performed in order to check for radiation damage. The data were normalized to the intensity of the incident beam; the scattering of the buffer was subtracted and the difference curves were scaled for concentration. Data processing was performed using the program package PRIMUS (Konarev et al., 2003). The forward scattering *I(0)* and the radius of gyration *Rg* were evaluated using the Guinier approximation (Guinier, 1939) assuming that at very small angles $(s < 1.3/R_g)$ the intensity is represented by $I(s) = I(0) \, exp(-(sR_g)^2/3)$. These parameters were also computed from the entire scattering patterns using the indirect transform package GNOM (Svergun, 1992), which also provide the distance distribution function *p(r)* of the particle ($p(r){=}2\pi \int I(s)sr\sin(sr)ds$). The molecular mass of ALIX$_{Bro1-V}$ and ALIX$_{Vmut1}$ were calculated by comparison with the forward scattering from the reference solution of bovine serum albumin (BSA). From this procedure a relative calibration factor for the molecular mass (MM) can be calculated using the known molecular mass of BSA (66kDa) and the concentration of the reference solution.

Low-resolution models of monomeric ALIX$_{Bro1-V}$, dimeric ALIX$_{Bro1-V}$ and monomeric ALIX$_{Vmut1}$ were built by the program DAMMIN (Svergun, 1999), which represents the protein as an assembly of dummy atoms inside a search volume defined by a sphere of the diameter D$_{max}$. Starting from a random model, DAMMIN employs simulated annealing to build a scattering equivalent model fitting the experimental data $I_{exp}(s)$ to minimize discrepancy:

$$\chi^2 = \frac{1}{N-1}\sum_j \left[\frac{I_{exp}(s_j) - cI_{calc}(s_j)}{\sigma(s_j)}\right]^2$$

where N is the number of experimental points, c a scaling factor and $I_{calc}(s_j)$ and $\sigma(s_j)$ are the calculated intensity and the experimental error at the momentum transfer s_j, respectively. Ten independent DAMMIN bead models for monomeric and dimeric $ALIX_{Bro1-V}$ and for $ALIX_{Vmut1}$ were calculated. Final models of these proteins were obtained by superposition of the ten independent shape reconstructions for each protein by using the program packages DAMAVER (Volkov and Svergun, 2003) and SUBCOMP (Kozin and Svergun, 2001). For dimeric $ALIX_{Bro1-V}$ *ab initio* shape models were calculated either without symmetry constrains or assuming a 2-fold symmetry axis. For the symmetric models, ten DAMMIN models were obtained, superimposed and averaged. The overall envelope, especially the crescent-shape of dimeric $ALIX_{Bro1-V}$ was the same for both unconstrained and constrained models.

References

Guinier, A. (1939). La diffraction des rayons X aux tres petits angles; application a l'etude de phenomenes ultramicroscopiques. Ann Phys (Paris) *12*, 161-237.

Konarev, P. V., Volkov, V. V., Sokolova, A. V., Koch, M. H. J., and Svergun, D. I. (2003). PRIMUS- a Windows-PC based system for small-angle scattering data analysis. J Appl Crystallogr *36*, 1277-1282.

Kozin, M. B., and Svergun, D. I. (2001). Automated matching of high- and low-resolution structural models. J Appl Crystallogr *34*, 33-41.

Lata, S., Roessle, M., Solomons, J., Jamin, M., Gottlinger, H. G., Svergun, D. I., and Weissenhorn, W. (2008). Structural basis for autoinhibition of ESCRT-III CHMP3. J Mol Biol *378*, 818-827.

Strack, B., Calistri, A., Popova, E., and Gottlinger, H. (2003). AIP1/ALIX is a binding partner for HIV-1 p6 and EIAV p9 functioning in virus budding. Cell *114*, 689 - 699.

Svergun, D. I (1992) Determination of the regularization parameter in indirect transform methods using perceptual criteria. J. appl. Crystallogr. *25*, 495-503.

Svergun, D. I. (1999). Restoring low resolution structure of biological macromolecules from solution scattering using simulated annealing. Biophys J *76*, 2879-2886.

Volkov, V. V., and Svergun, D. I. (2003). Uniqueness of ab initio shape determination in small-angle scattering. J Appl Crystallogr *36*, 860-864.

Supplementary Figures

Figure S1:
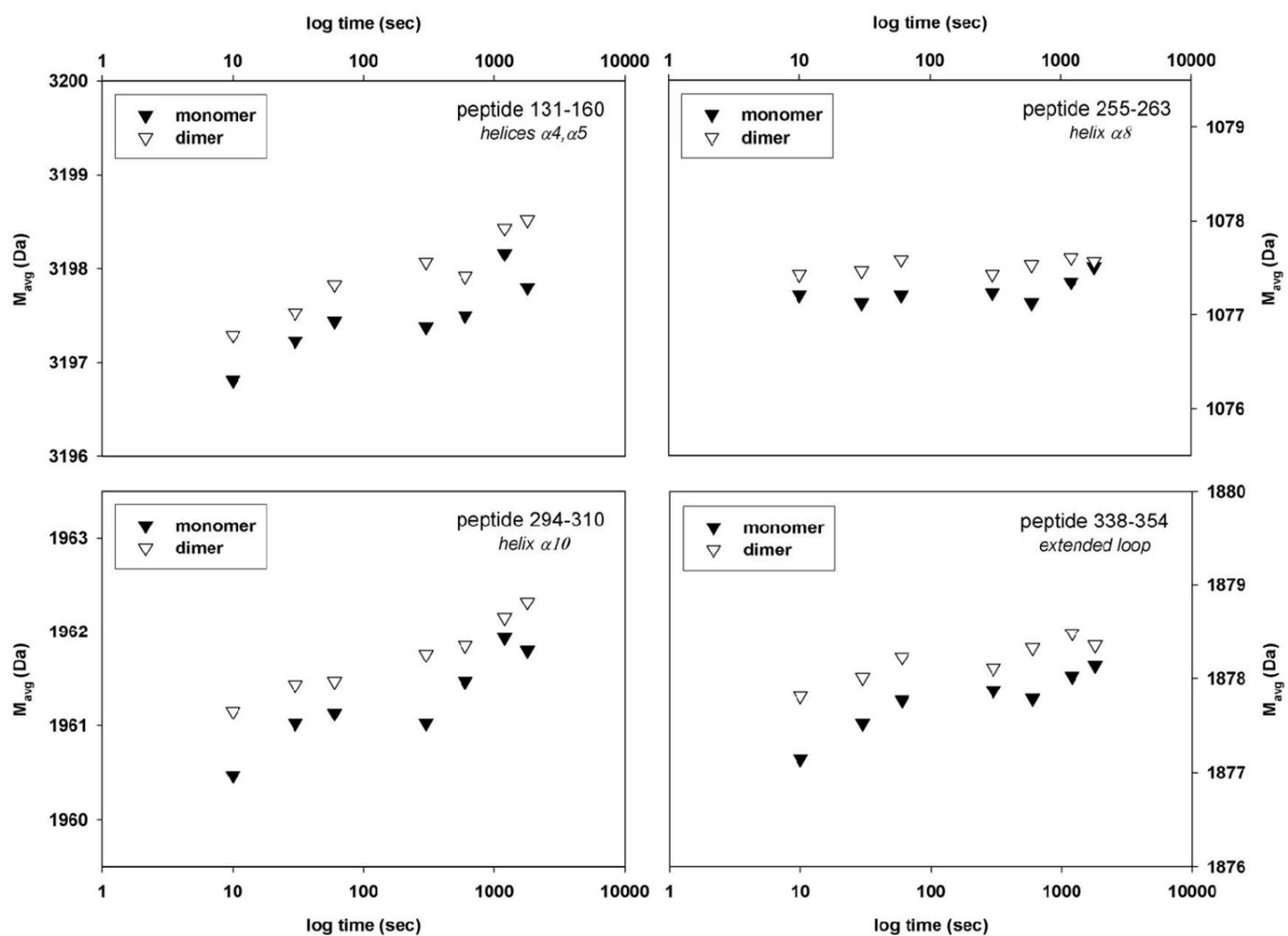
Local H/D exchange kinetic for peptides derived from the Bro1 domain. The average mass is plotted against the D_2O incubation time. These peptide regions demonstrate an increase in deuterium exchange in the $ALIX_{Bro1-V}$ dimer as compared to the monomer.

Figure S2
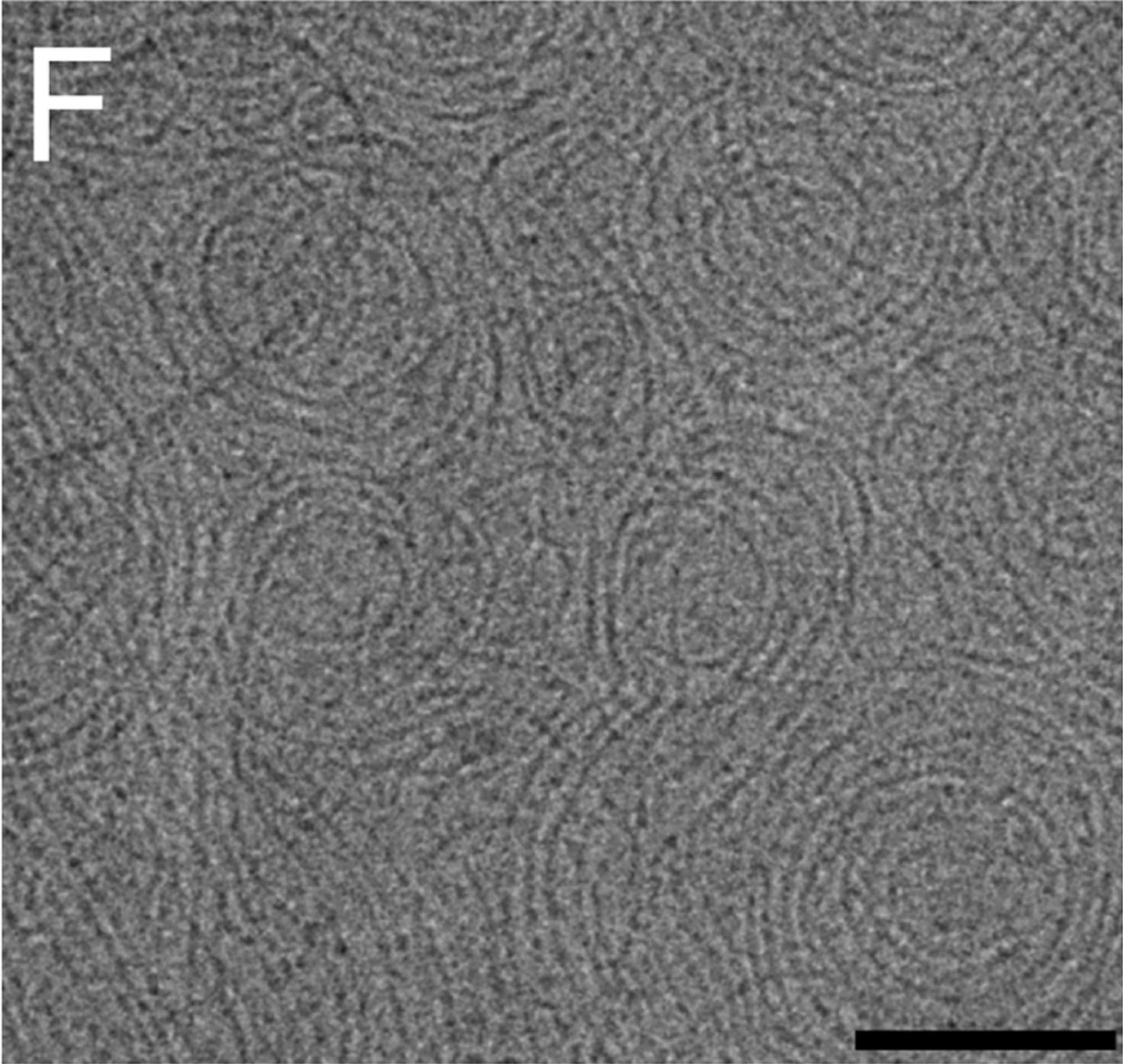
Cryo EM image of CHMP4B$_{\Delta C\text{-ALIX}}$. Magnification of figure 9F. Scale bar is 100 nm.

Figure S3
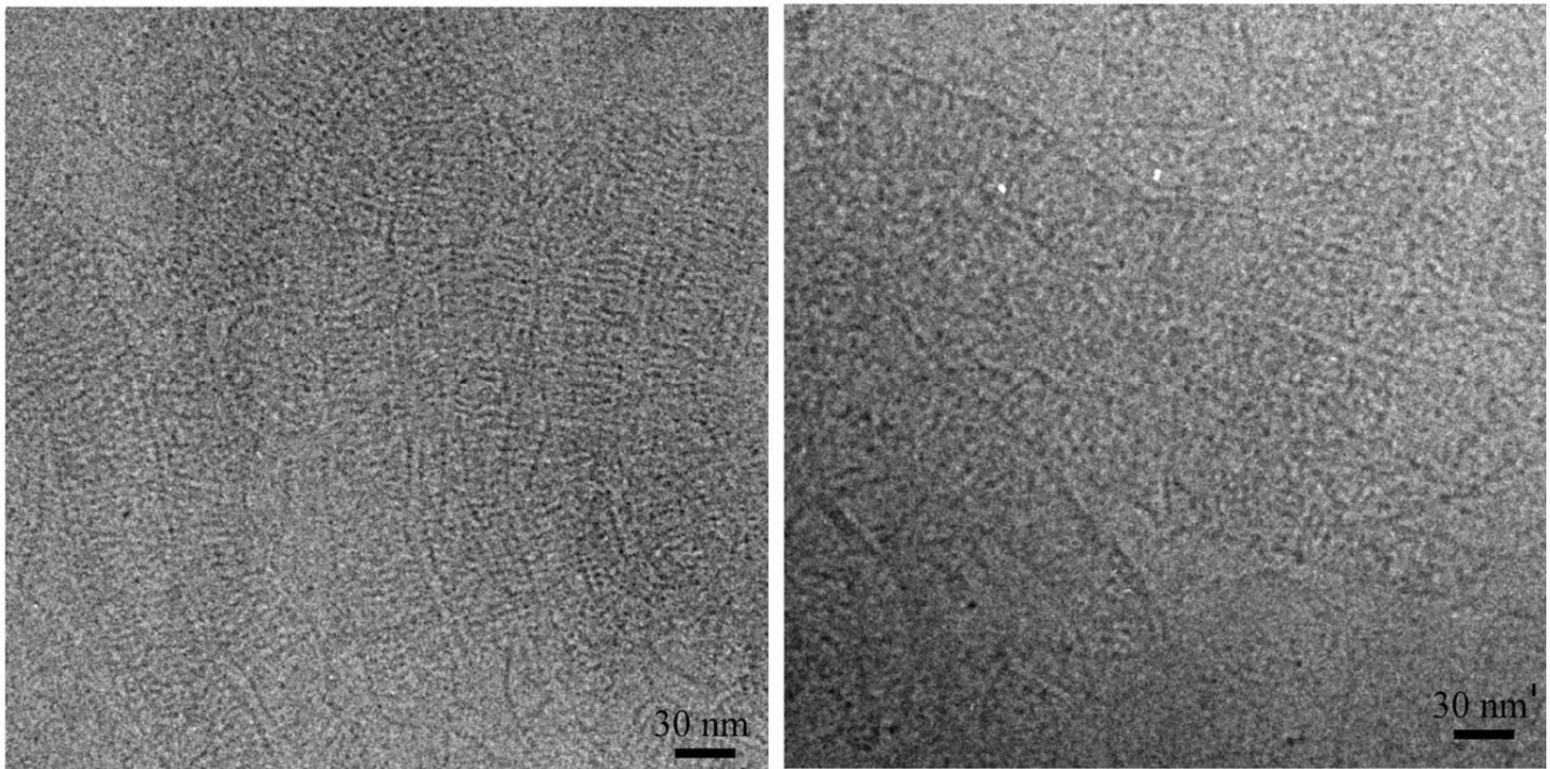
Cryo EM images of CHMP4B$_{\Delta C\text{-}ALIX}$ - ALIX$_{Bro1\text{-}V}$ (dimer) complexes revealing mostly ladder-like structures.